Doctoral Thesis

Photo-healable Ion Gels Using Tetra-arm Diblock Copolymers Containing Azobenzene Group

(アゾベンゼン基を有する４分岐型ジブロック共重合体を用いたイオンゲルの光治癒)

Graduate School of Engineering

Yokohama National University

(国立大学法人 横浜国立大学大学院 工学府)

Xiaofeng Ma

(暁峰 馬)

December 2015

Photo-healable Ion Gels Using Tetra-arm Diblock Copolymers

Containing Azobenzene Group

A Dissertation Submitted to Yokohama National University

for the Partial Fulfillment of the Requirements for the

Degree of Doctor of Engineering

Submitted by

Xiaofeng Ma

12SA593

December 2015

Department of Materials Science and Engineering

Specialization in Advanced Materials Chemistry

Yokohama National University

Yokohama, Japan

Contents

Acknowledgements

I would like to express my deepest gratitude and sincere appreciation to my supervisor **Professor Masayoshi Watanabe**, Department of Chemistry and Biotechnology, Yokohama National University, Japan, for his extraordinary patience, consistent encouragement, scholastic supervision and invaluable guidance throughout the course of the present work. I appreciate a lot for helping me with application of scholarship and giving me an opportunity to study here. But for his great help, I would not have accomplished this thesis.

I am truly grateful to **Dr. Hisashi Kokubo**, Department of Chemistry and Biotechnology, Yokohama National University, Japan, for his encouraging suggestion and inspiration during this work and his help in application of scholarship and complicated procedure of admission before enrollment.

I would like to express my gratitude to **Professor Masayoshi Watanabe**, **Professor Kazuyoshi Ueda**, **Professor Mahito Atobe**, **Professor Toshiyuki Oyama** and **Professor Takashi Ubukata** for their constructive suggestions as members of the examining committee.

I am greatly indebted to **Dr. Yuzo Kitazawa** for his encouraging suggestions, revising my paper, giving invaluable advice on my research and helping me in various aspects during these years. Without his help, I could not have studied here smoothly.

I am very grateful to **Dr. Morgan L. Thomas** for revising my paper and giving me useful advices. I would like to express deep gratitude to **Professor Tomohiro Yasud**a, **Dr. Kazuhide Ueno**, **Dr. Shiguo Zhang**, **Dr. Zhengjian Chen** and **Dr. Yutaro Kamei** for their instructive suggestions and encouragements in the past three years.

Special thanks should go to **Mr. Shota Sawamura**, **Mr. Ryoji Usui**, **Mr. Syuntai Ishi and Ms. Yumi Kobayashi** for their help in polymerization methods and characterization of polymers, enlightening instructions and fruitful discussions during the course of the present work.

I very appreciate **Dr. Ce Zhang** and **Mr. Jiazhi Wang** for their generous help and

Abstract

Photo-healable ion gels have been developed by utilizing photo-induced sol-gel transition of thermo-sensitive triblock copolymer in an ionic liquid (IL). They are particularly appealing, as the use of light as stimulus for healing provides several advantages such as controlled healing in a non-contact way and locally delivered stimulus only to damaged parts. In addition, unique properties of IL remained. However, lower mechanical properties that result from network defects including loops and dangling end chains formed in gelation process, which may limit its application in some fields. Therefore, it is of particular interest to develop a photo-healable ion gel with higher mechanical properties to expand its application.

Herein, a tetra-arm diblock copolymer (A(B)$_4$: [PEG-*b*-P(AzoMA-*r*-NIPAm)]$_4$) was synthesized by reversible addition-fragmentation chain transfer (RAFT) copolymerization of *N*-isopropylacrylamide (NIPAm) and 4-phenylazophenyl methacrylate (AzoMA), initiating from the ends of functionalized tetra-arm polyethylene glycol (tetra-PEG). The resulting tetra-arm diblock copolymer consists of two segments: tetra-PEG as A block (the center block; compatible with 1-butyl-3-methylimidazolium hexafluorophosphate ([C$_4$mim]PF$_6$)) and P(AzoMA-*r*-NIPAm) as B block (the end blocks; temperature- and photosensitive compatibility with [C$_4$mim]PF$_6$ due to photoresponsive upper critical solution temperature (UCST) phase behavior). We also prepared a triblock copolymer (A(B)$_2$) (A block: PEG, B block: P(AzoMA-*r*-NIPAm)) for comparison.

We found that A(B)$_4$ and A(B)$_2$ polymers in [C$_4$mim]PF$_6$ with diluted conditions underwent high-temperature unimer and low-temperature micelle (upper critical micellization temperature (UCMT)) transitions. The UCMT of the both polymers

depended on photoisomerization states of the azobenzene groups within the copolymer. The UCMT of the *trans*-form polymer in dark conditions was higher than that of the *cis*-form polymer under UV-light irradiation. We demonstrated photoinduced self-assembly changes of the both polymers in [C_4mim]PF_6 at a bistable temperature. Reversible photoinduced unimer/micelle transitions were also demonstrated.

We also compared gelation properties of A(B)$_4$ ion gels and A(B)$_2$ ion gels at different concentration. It is found that the A(B)$_4$ ion gels have higher modulus and less network defects, as compared with A(B)$_2$ ion gels. Self-standing A(B)$_4$ ion gels were obtained at a lower polymer concentration in [C_4mim]PF_6 than the A(B)$_2$ ion gels in the same ionic liquid. The A(B)$_4$/[C_4mim]PF_6 binary system exhibits low temperature gel-state and high temperature sol-state, i.e., gel-to-sol transition with increasing temperature, due to UCST-type phase behavior of the B block. The gel-to-sol transition temperatures also depend on photoisomerization states of the azobenzene moiety in the polymers. It is found that photo-induced sol-gel transition is reversible at a suitable temperature. Photo-healable ion gels are proposed by the utilization of the photo-induced reversible sol-gel transition, i.e., damaged parts of the gels are UV-light-irradiated to induce the gel-to-sol transition, followed by visible-light irradiation to heal the gels by the sol-to-gel transition. Remarkable photo-healing efficiency in terms of the mechanical properties is realized by this healing procedure.

Chapter 1 Introduction

1.1 Ionic liquids

Ionic liquids (ILs) are ambient temperature molten salts.[1] The first IL is Ethanolammonium nitrate with melting point of 52-55 °C, which was reported in 1888 by Gabriel.[2] The first room temperature ionic liquids is ethyl ammonium nitrate ([EtNH$_3$][NO$_3$]), reported by Walden in 1914,[3] which has a melting point of 13-14 °C. However, ILs have attracted little attention from scientists for a long time afterwards. The interest in studies on room temperature ILs was newly attracted since the discovery of dialkylimidazolium chloroaluminate ionic liquids made from mixtures of aluminum chloride and 1,3-dialkylimidazolium chloride in 1982,[4] although it is sensitive to moisture. The air- and water-stable ionic liquids with alkylimidazolium-based cations and tetrafluoroborate (BF$_4^-$) or nitrate (NO$_3^-$) anions were firstly reported in 1992,[5] after that the increase in scientific interest for ionic liquids has become very fast.[6]

ILs are composed entirely of cations and anions. ILs are also considered as "designer solvents" or "the third solvents", following conventional water and organic solvent, owing to infinite number of combinations of cations and anions. There are many known and potential cations and anions structures. Common IL cations include 1-alkyl-3-methylimidazolium (C$_n$mim), *N*-methyl-*N*-ethyl-pyrrolidinium (P12), *N*-alkyl-pyridine (C$_n$py), and alkylammonium (trimethyl-butylammonium: N$_{1114}$), IL anions can be selected from a broad range of inorganic anions including halides (Cl$^-$,

Br$^-$. I$^-$) and polyatomic inorganics (tetrafluoroborate (BF$_4^-$), hexafluorophosphate

(PF$_6^-$)) or organic anions such as bis(trifluoromethylsulfonyl)amide (NTf$_2$),

bis(pentafluoroethanesulfonyl)amide (BETI) and trifluoromethanesulfonate (TfO)

(**Figure 1.1**). Compared with conventional inorganic salts, such as sodium chloride

and potassium chloride, ionic liquids have much lower melting points, because the

ions of ionic liquids are typically bulky, irregularly shaped, and with delocalized

charge. These characteristics suppress formation of well-ordered crystal lattices,

resulting in much lower melting points.
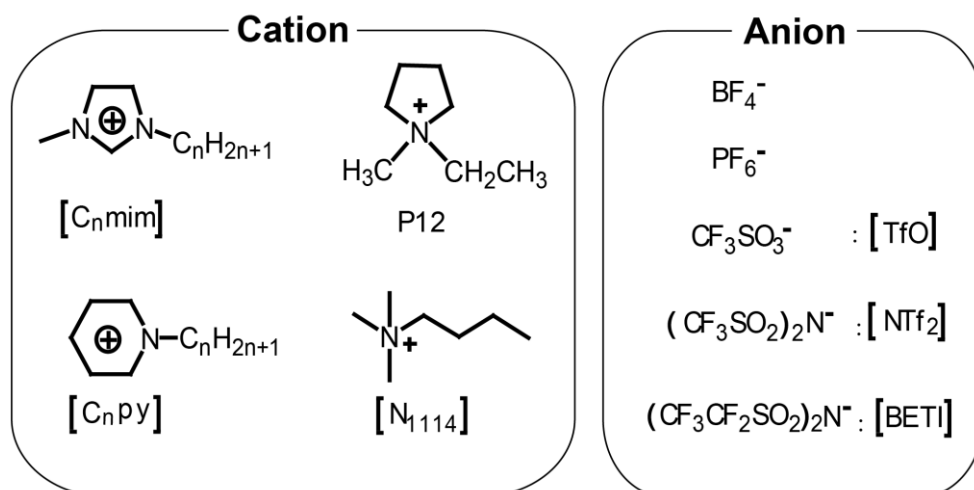
Figure 1.1 Typical organic cations and counter anions which form ionic liquids.

Physicochemical properties of ILs are one of the primary reasons to attract so much

interest from scientist, such as negligible vapor pressure, low flammability, thermal

stability, chemical stability and high ionic conductivity.[7] Negligible vapor pressure

(as low as 10^{-10} Pa at 25 °C) provide possibility to directly introduce them into

analytical instruments requiring high vacuum conditions,[8] such as X-ray

photo-spectroscopy (XPS), transmission electron microscopy (TEM) and

matrix-assisted laser desorption/ionization (MALDI) mass spectroscopy. For instance, polymeric nanostructures in ionic liquid solutions can be simply observed by using room temperature conventional TEM,[9] in contrast to cryogenic TEM, which involves a complicate sample preparation process.[10] High ionic conductivity, low flammability and negligible vapor pressure of ILs make them possible to prepare polymer gel electrolytes without issues of organic solvent-based electrolytes such as leakage and flammability.[11] Moreover, the remarkable electrochemical properties of ionic liquids, such as high ionic conductivity (up to 100 mS/cm) and wide electrochemical windows (typically 4-6 V), make them have diverse electrochemical application such as electronic double layer capacitors,[12] fuel cells,[13] lithium ion batteries,[14] and solar cells.[15] Furthermore, physicochemical properties of ionic liquids can be tuned by variation combinations of cations and anions. For example, we reported a series of 1,3-dialkylimidazolium-based ionic liquids on their physical properties, such as density, viscosity, self-diffusion coefficient, thermal behavior, and ionic conductivity, can be changed by varying cationic[16]/ anionic[17] species and alkyl chain length.[18]

It is interesting to note that ILs can be good solvents for many synthetic polymers and many natural polymers, which provide possibility to process these polymers that is reluctant to dissolve in conventional solvents. For example, Poly (acryloylmorpholine) is known to be incompatible with many kinds of organic solvents, but it can readily dissolve in certain ILs, such as 1-ethyl-3-methylimidazolium bis(trifluoromethanesulfonyl)amide ($[C_2mim][NTf_2]$) and 1-butyl-3-methylimidazolium hexafluorophosphate ($[C_4mim]PF_6$). For

biopolymers, the most famous example is the use of ionic liquids as solvents for cellulose processing, which was first reported by Rogers and co-workers.[19] Based on this concept, solubilization of other natural polymers in ILs, such as silk,[20] wool,[21] keratin,[22] and chitin,[23] also is studied. ILs can also be used as solvent for synthesis and catalysis.[24] For instance, we reported that vinyl monomers can polymerized in 1-ethyl-3-methylimidazolium tetrafluoroborate ([C_2mim]BF_4) and 1-butylpyridinium tetrafluoroborate ([C_4py]BF_4).[25] For biphasic catalysis, ionic liquids can be utilized as one phase for establishment of biphasic systems; the other phase is organic solvents or water. In such system, catalysts are immobilized in one phase while products are readily separated from the other phase, whereby combination of the merits of homogeneous catalysis (high catalytic performance) with the advantages heterogeneous catalysis (facile product separation and catalyst recycling) can be realized.[26] Ionic liquids have also been widely employed in separation technology, such as liquid-liquid extractions and supported liquid membranes.[27]

1.2 Phase behavior of polymers in ionic liquids

As mentioned above, ionic liquids can be good solvents for many synthetic polymers. However, certain polymers in ILs exhibit phase separation induced by thermal or light. Such polymers/ILs systems are of particular interest, because phase separation of these polymers in nonvolatile and thermal-stable ILs can realize many useful smart materials. In general, there are two kinds of cases for thermo-sensitive polymers. The first case is that polymer becomes soluble blow a critical solution temperature which is so-called lower critical solution temperature (LCST). The other

case is that reverse phenomena occur, and the critical solution temperature named upper critical solution temperature (UCST). From the thermodynamic point of view, for mixture of polymer and IL, when the Gibbs free energy of mixing (ΔG_{mix}) of the polymer and IL is negative, suggesting polymer is compatible with IL.

$$\Delta G_{mix}=\Delta H_{mix}-T\Delta S_{mix} \tag{1.1}$$

where ΔH_{mix}, T, and ΔS_{mix} are the enthalpy of mixing, absolute temperature, and entropy of mixing, respectively.

For polymer in IL shows LCST-type phase behavior, both ΔH_{mix} and ΔS_{mix} should be negative (**Figure 1.2a**). At lower temperature, ΔG_{mix} is negative, indicating polymer is compatible with IL; when the entropic term ($-T\Delta S_{mix}$) exceeds the enthalpic term (ΔH_{mix}) with increasing temperature, desolvation of the polymer happens, resulting in LCST phase separation. Conversely, for UCST-type polymers in IL, both ΔH_{mix} and ΔS_{mix} should be positive (**Figure 1.2b**). At lower temperature, ΔG_{mix} is positive, indicating polymer is incompatible with IL; ΔG_{mix} become negative with increase of temperature, demonstrating polymer is soluble in IL.
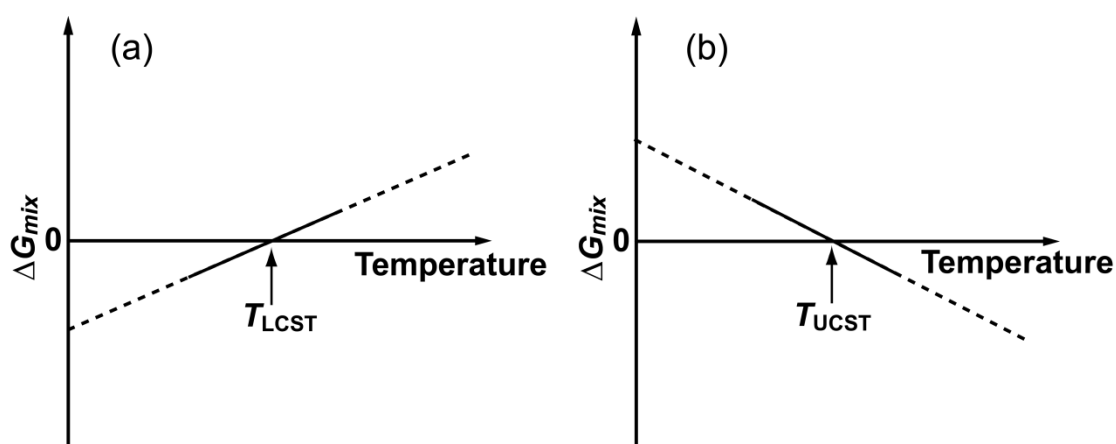
Figure 1.2. Relationship between the Gibbs free energy of mixing (ΔG_{mix}) and temperature for LCST (a) and UCST (b) phase behavior.

Previously, we reported for the first time that poly(benzyl methacrylate) (PBnMA) showed LCST-type phase behavior in $[C_2mim][NTf_2]$, as shown in **Figure 1.3**, where 100% transmittance suggests a transparent solution, in which polymer is soluble in IL, whereas transmittance <100% indicates the solution is turbid, which means phase separation occurs. As mentioned above, for binary polymer/solvent systems of the LCST-type phase behavior, the essential requirements are a negative ΔS_{mix} as well as a negative ΔH_{mix} (exothermic) in **equation 1.1**. In other words, exothermic and structure-forming solvation must be existence. Even though it is still unclear that what factors lead to the decrease in entropy for mixture of PBnMA and IL; there are some reports on the formation of structurally ordered aggregates in aromatic compounds/ILs binary system,[28] for instance, the so-called "liquid clathrates". Therefore, this ordered structure causes a negative ΔS_{mix}. A negative ΔH_{mix} is induced by the interaction between the ester group and the IL. Thus, thermodynamic requirements of LCST-type phase separation can be satisfied, because both conditions are essential for the appearance of LCST-type phase separation of this polymer in ILs. In addition to PBnMA, poly(*n*-butyl methacrylate) (P(nBMA)),[29] poly(ethylene oxide) (PEO) and its derivatives[30, 31] also exhibit LCST-type phase behavior in certain ILs. One unusual feature of PEO system is the asymmetry of cloud point curves in the temperature-composition phase diagrams, and the critical composition shifted to high concentrations of PEO. Conversely, for temperature-composition phase diagrams of P(nBMA), and the critical composition shifted to low concentrations of P(nBMA).
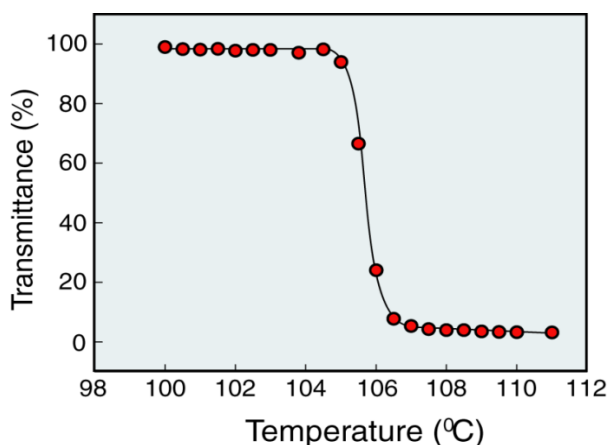
Figure 1.3. Temperature dependence of transmittance at 500 nm for 3 wt% Poly (benzyl methacrylate)/[C$_2$mim][NTf$_2$] solution.

UCST-type phase behavior of poly(*N*-isoproylacrylamide) (PNIPAm) in [C$_2$mim][NTf$_2$] was first reported by our group.[32] This behavior is of very interest, because it is completely opposite phenomenon as that shows in aqueous media. UCST of PNIPAm depends strongly on both the concentration and molecular weight of polymer (**Figure 1.4**). **Figure 1.5** shows the relationship between the UCST of PNIPAm and the donor number (DN) of ILs. PNIPAm which was prepared by RAFT polymerization has a relatively narrow polydisperisity index (PDI). It is apparent that the UCST of PNIPAm in the ILs decreased with increasing the DN. This result is consistent with a report on UCST of PNIPAm in a variety of organic solvents having different donor number increases with a decrease in the DN.[32]
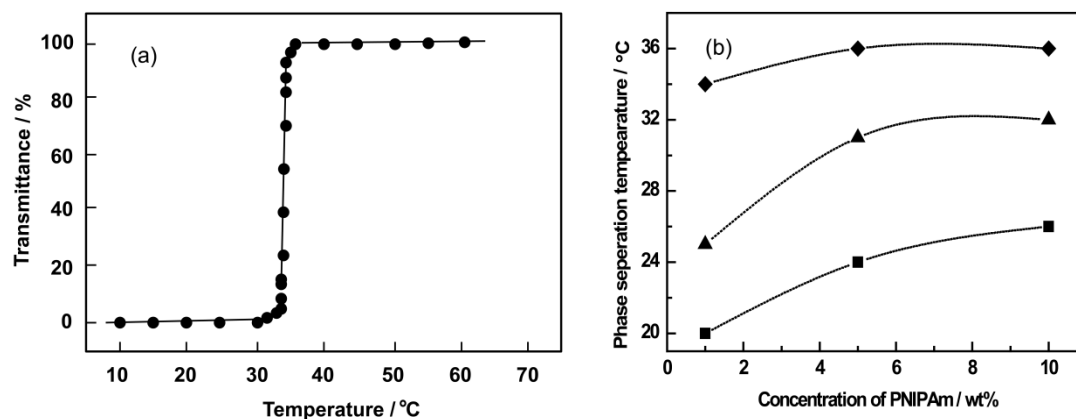
Figure 1.4. Temperature dependence of transmittance at 500 nm for 1 wt% poly(N-isopropylacrylamide) (PNIPAm) solution in [C_2mim][NTf$_2$] with a cooling rate of 0.5 °C/min (a). Relationship between UCST phase separation temperatures of PNIPAm in IL and concentrations of PNIPAm (b). (squares: M_n = 15400 g/mol, PDI = 1.64, triangles: M_n = 38900 g/mol, PDI = 2.17, diamonds: M_n = 52300 g/mol, PDI = 2.62).
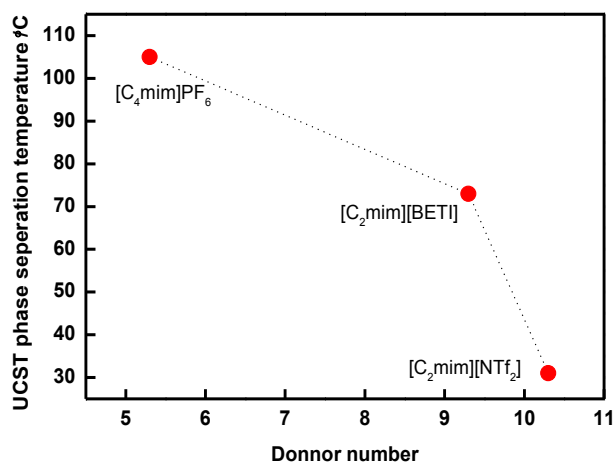
Figure 1.5. Relationship between UCST of 3 wt% Poly(N-isopropylacrylamide) (M_n = 40 kDa, PDI = 1.19) solutions in indicated ILs and the solvent donor number.

Photo-responsive polymers in ionic liquids have also been reported by our group. We previously reported a random copolymer of 4-phenylazophenyl methacrylate (AzoMA) and benzyl methacrylate (BnMA) (P(BnMA-*r*-AzoMA)) exhibits a LCST-type phase behavior in [C$_2$mim][NTf$_2$]. LCST difference between the *trans*-polymer and *cis*-polymer was as large as 22 °C, when azobenzene content within copolymers was 4.1 mol%.[33] We also reported a random copolymer of AzoMA and NIPAm (P(AzoMA-*r*-NIPAm)) shows UCST-type phase behavior in [C$_2$mim][NTf$_2$].[34] **Figure 1.6** shows UCST phase separation temperature of P(AzoMA-*r*-NIPAm) depended on photo-isomerization states of azobenzene in copolymers. UCST difference (ΔT_c) between *trans*-polymer and *cis*-polymer increased with increase of azobenzene content in copolymers. UCST of *trans*-polymers is higher than that of *cis*-polymers. This temperature difference is ascribed to polarity difference between *trans*- and *cis*-form azobenzene. At a suitable temperature, photo-induced phase separation was reversible (**Figure 1.7**). It is worth noting that ΔT_c is strongly affected by different IL, for example, **Figure 1.6** shows that ΔT_c of P(AzoMA-*r*-NIPAm) with azobenzene content of 8.6 mol% was 8 ℃ in [C$_2$mim][NTf$_2$], however, we reported ΔT_c of the same polymer was approximately 24 ℃ in [C$_4$mim]PF$_6$.[35]
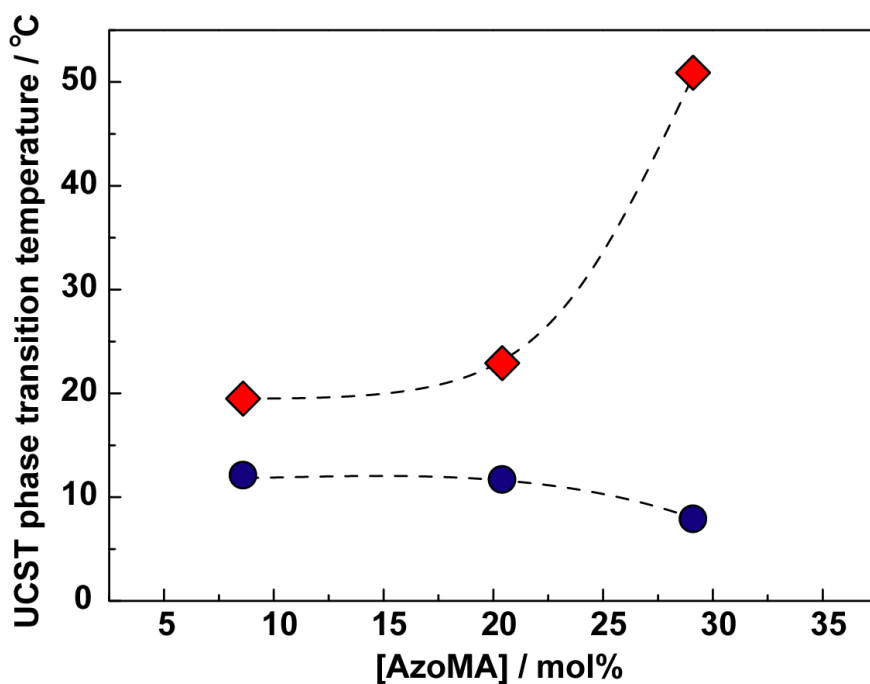
Figure 1.6. Relationship between UCST phase separation temperature (T_c) of P(AzoMA-*r*-NIPAm) under dark (red diamonds) and UV light irradiation (blue circles) and AzoMA composition in the random copolymers. T_c was determined as the temperature of 50% transmittance.
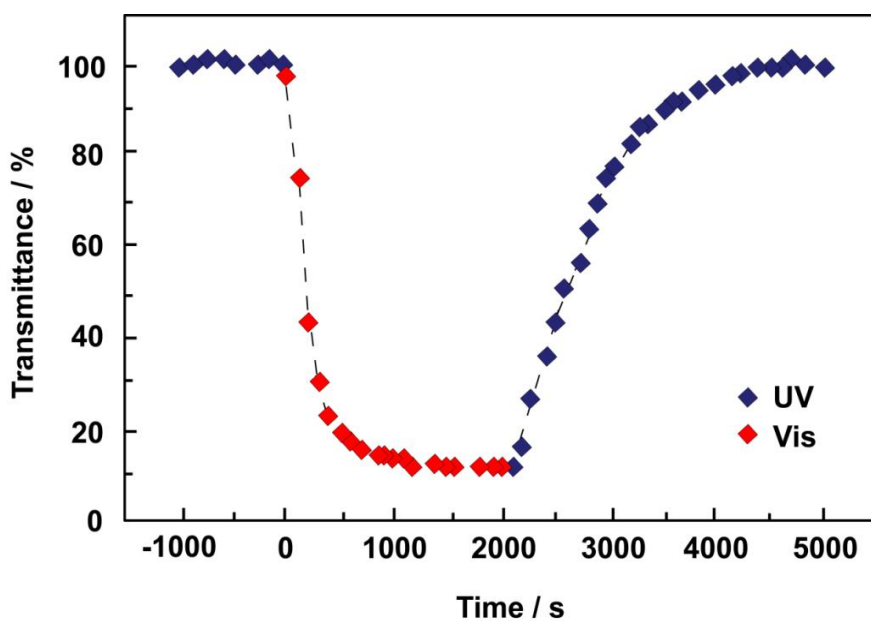
Figure 1.7. Photoinduced phase transition of P(AzoMA$_{8.6}$-*r*-NIPAm) with visible light (red squares) or UV light (blue squares) irradiation at 15.8 $^{\circ}$C in [C$_2$mim][NTf$_2$].

1.3 Self-assembly of block copolymers in ionic liquids

1.3.1 Block copolymers

Block copolymers are macromolecules which formed by the coupling of two or more chemically distinct polymer segments (blocks) in a linear and/or radial arrangement. Self-assembly of block copolymer is of great interest, because many ordered microstructures can be obtained from the self-assembly of block copolymer in solution or bulk state, due to microphase separation that induced by immiscibility between connected blocks. In dilute solution, block copolymers will form micelles when the solvent is selective for one of blocks, micelle morphologies include spheres, cylinders, and vesicles, and so forth. In concentrated solution or bulk state, these microstructures have cubic, hexagonal, and layered architectures, and so on.[36] These architectures generally have sizes of 5-50 nm, which is difficult to achieve by conventional lithography.[37] Thus, Spontaneous self-assembly of block copolymers has been considered as a novel bottom-up strategy for nano-patterning techniques.[38] Block copolymers self-assemblies have also been applied in many other fields such as drug delivery,[39] nanoreactor,[40] templates for nanoporous or mesoporous materials,[41] Photonic crystals,[42] and holography,[43] and so on. In addition, block copolymers with quite complicated architectures can be straightforward synthesized by using living radical polymerization methods, such as atom-transfer radical polymerization (ATRP),[44] reversible addition fragmentation transfer polymerization (RAFT)[45] and nitroxide-mediated polymerization (NMP),[46] due to advancement of highly controlled living polymerization techniques.

1.3.2 Dilute solutions of block copolymers in ionic liquids

Self-assembly of block copolymers in ionic liquids has also been developed in the past decade. Many well-defined nanostructures can also be achieved by self-assembly of block copolymers in ILs. Compared to nanostructures in aqueous media or organic solvents, such nanostructures in ILs have the merits of long-term stability, due to nonvolatility and thermal stability of ILs. In dilute solution, not unlike block copolymer in other solvents, a variety of micelles also are formed in ILs, such as, spherical micelles, cylindrical micelles, vesicles. For example, Lodge and coworkers reported that diblock copolymers poly(butadiene-*block*-ethylene oxide) (PB-*b*-PEO) form micelles of a PB-core surrounded by a PEO-shell in a hydrophobic IL, 1-butyl-3-methylimidazolium hexafluorophosphate ($[C_4mim]PF_6$).[47] The morphology of micelles can be changed from spherical micelles, cylindrical micelles to bilayer vesicles by varying the chain length of PEO block (**Figure 1.8**). This phenomenon is consistent with that in aqueous and organic systems, in which the micellar structures progresses from spheres to cylinders to vesicles through decreasing the volume fraction of the solvatophilic blocks. Further investigation of these polymers by Lodge and coworkers result in discovery of "micelle shuttle" which is thermo-reversible intact micelles shuttling between water and a hydrophobic ionic liquid, 1-ethyl-3-methylimidazolium bis(trifluoromethylsulfonyl)imide ($[C_2mim][NTf_2]$).[48,49] The most remarkable characteristic of this micelle shuttle system is complete transference of the micelles between water and ILs, without involving dissociation-reassembly process. This simple round-trip delivery system is of

particular interest in transporting nonpolar reagents, products, or byproducts quantitatively into and out of the ionic liquids, without removing the expensive ionic liquids from the reaction vessel.
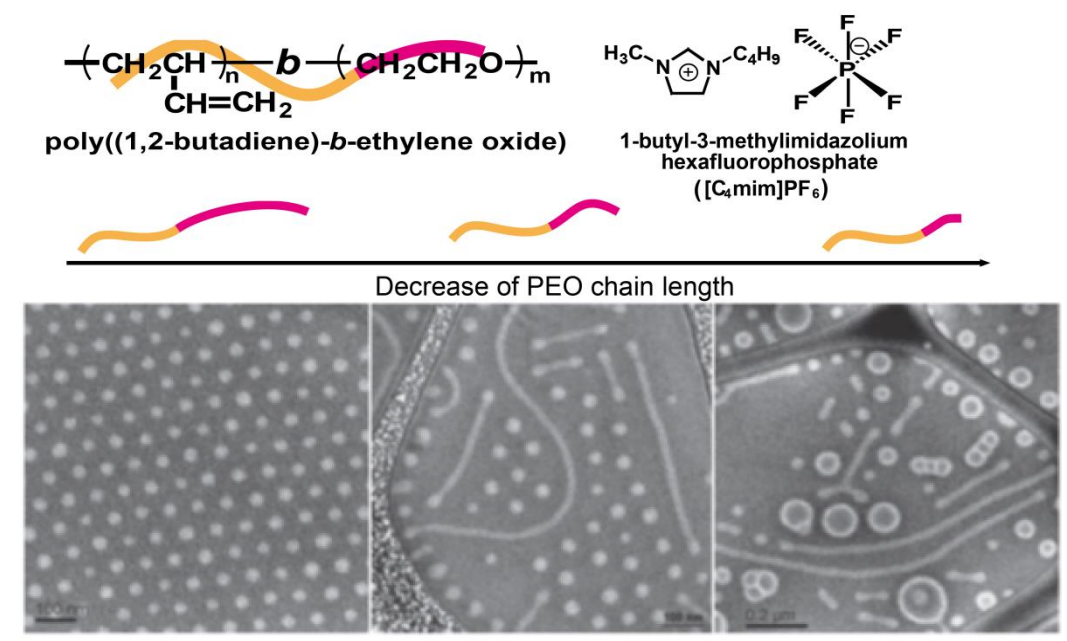
Figure 1.8. Schematic illustration of poly((1,2-butadiene)-*b*-ethylene oxide) (PB-*b*-PEO) and [C$_4$mim]PF$_6$ (upper). Cryo-TEM images for self-assembly of PB-*b*-PEO in [C$_4$mim]PF$_6$ (bottom). White dots (left), white strings (center), and white double circles (right) correspond to spherical micelles, cylindrical micelles, and bilayer vesicles, respectively.

Stimuli-responsive block polymer/ionic liquid system have also been utilized to develop stimuli-responsive micelles including thermo-induced micelles and thermo-/photo-induced micelles. Our group reported a poly(benzylmethacrylate-*b*-methylmethacrylate) (PBnMA-*b*-PMMA)) exhibited low-temperature unimers and high-temperature micelles in a hydrophobic IL

[C$_2$mim][NTf$_2$], due to LCST-type phase behavior of P(BnMA) segment and solvatophiliciy of PMMA segment.[50] Lodge and coworker also reported that low-temperature free chains and high temperature micelles of poly(n-butyl methacrylate-b-ethylene oxide) (PnBMA-b-PEO) diblock copolymer in an IL, thanks to LCST-type phase behavior of PnBMA.[51,52]

Another interesting example is that block copolymer can respond to more than one temperature change. For example, we prepared a doubly thermosensitive block copolymer consisting of a LCST PBnMA segment and an UCST PNIPAm segment that exhibit thermo-induced micelle-unimer-inverse micelle transition in an IL [C$_2$mim][NTf$_2$].[53] At temperatures below the UCST of the PNIPAm segments and LCST of the PBnMA segments, micelles with PNIPAm-core surrounding by PBnMA-shell are formed. In contrast, at temperatures higher than the LCST of PBnMA blocks and UCST of PNIPAm blocks, micelles comprising PBnMA-core and PNIPAm-corona are formed (**Figure 1.9**). Similar phenomenon also be observed by Lodge and coworker by using block copolymer PNIPAm-b-PEO in a mixture of [C$_2$mim][BF$_4$] and [C$_4$mim][BF$_4$].[54]

18
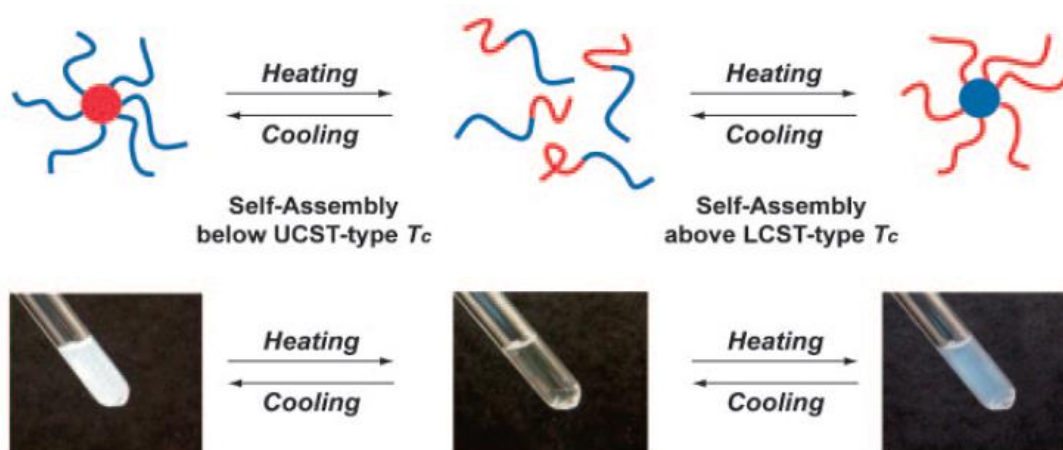
Figure 1.9. Conceptual illustration of doubly thermosensitive self-assembly of block copolymer in an IL (upper) and appearance of block copolymer/IL solution at different sample temperature (bottom).

Responsive block copolymer employing temperature and light as stimuli is of great interest, since light as a stimulus can be remotely controlled and localized to a specific location.[55] Thermo-/photo-induced self-assembly of block copolymer in an IL was first reported by our group.[35] In that report, an azobenzene containing diblock copolymer having PEO as IL-philic block and P(AzoMA-*r*-NIPAm) as thermo-/photo-responsive block (PEO-*b*-P(AzoMA-*r*-NIPAm)) exhibited thermo- and photo-induced micellization in [C$_4$mim]PF$_6$. The diblock copolymer formed micelles at lower temperatures than the UCST of P(AzoMA-*r*-NIPAm). Conversely, the block copolymer became unimers at higher temperatures than the UCST. The upper critical micellization temperature (UCMT) depended on the photoisomerization states of azobenzene in the copolymers. The UCMT difference between the *trans*-form polymer and the *cis*-form polymer was 4 °C. At a suitable temperature, photo-induced

reversible unimer/micelle transition was realized by alternate illumination of UV and visible light (**Figure 1.10**).
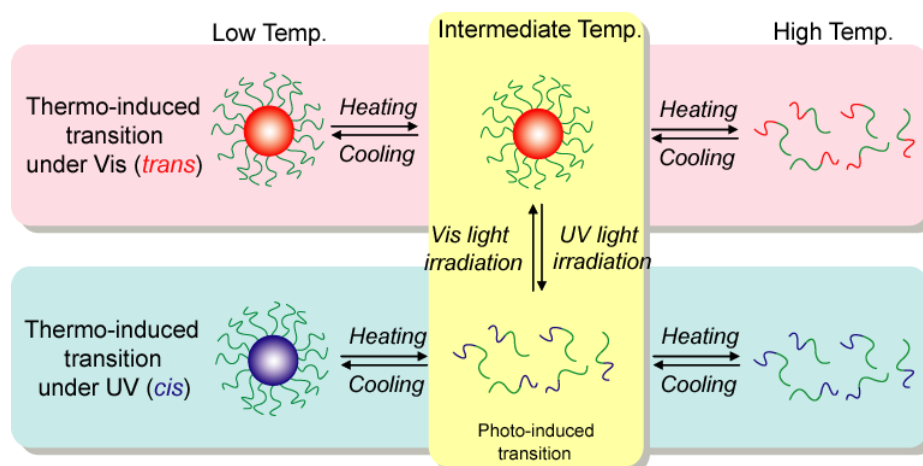
Figure 1.10. Conceptual illustration of doubly thermo-/photo-induced self-assembly of block copolymer PEO-*b*-P(AzoMA-*r*-NIPAm) in [C$_4$mim]PF$_6$.

1.3.3 Concentrated solutions of block copolymers in ionic liquids

Concentrated solutions of block copolymers in ionic liquids have even more diverse microstructures than dilute solutions. These microstructures formed by simple AB diblock copolymers generally include spheres packed onto body-centered-cubic lattices (SBCC), hexagonally packed cylinders (C), the bicontinuous gyroid (G), and lamellae (LAM). However, investigations of concentrated solutions are much less developed compared to that of dilute solution self-assembly.

Lodge and coworkers first reported that the lyotropic phase behavior of a series of poly(1,2-butadiene-*block*-ethylene oxide) diblock copolymers (PB-*b*-PEO) with different monomer volume fractions in two different ionic liquids, [C$_2$mim][NTf$_2$] and [C$_4$mim]PF$_6$ at different concentrations.[56] The results of small-angle X-ray scattering

(SAXS) indicated the ordered microstructures present in the solutions include SBCC, C, and LAM. In addition to these classical microstructures, there are coexistence regions between LAM and C, as well as a disordered network structure consisting of branched PB cylinders in a matrix of PEO/ionic liquid. G microstructure didn't occur from these systems at the relevant block copolymer and ionic liquid compositions. However, they developed another mixtures of diblock copolymers poly(styrene-*block*-ethylene oxide) (PS-*b*-PEO) with [C$_2$mim][NTf$_2$], which demonstrated coexistence between LAM, C, and G microstructures.[57] The coexistence of the G microstructure is of great interest because this morphology was not observed from the PB-*b*-PEO/[C$_2$mim][NTf$_2$] and PB-*b*-PEO/[C$_4$mim]PF$_6$ phase diagrams.

Other systems were also developed by other group. For example, Segalman and coworker reported a variety of morphologies can be formed by self-assembly of diblock copolymers poly(styrene-*block*-2-vinylpyridine) (PS-*b*-P2VP) in ILs.[58] In that report, a variety of morphologies, including lamellae, hexagonally close-packed, cylinders, body-centered cubic, face-centered cubic, and disordered PS micelles, can be obtained by adjusting volume fraction of one segment or varying polymer concentrations. The lamellae structure of PS-*b*-P2VP diblock copolymer and IL composite has been applied into photonic crystals, which has recently reported by Noro and coworkers.[59]

It is worth noting that triblock copolymer can also self-assemble into various micelles in ILs with dilute solutions and diverse order structures in ILs with

concentration solutions. However, most of investigations for self-assembly of triblock copolymer in ILs focus on development of ion gels, because of unique properties and diverse applications of triblock copolymer ion gels. Therefore, brief introduction of ion gels will be present in the following.

1.4 Ion gels

Ion gels are polymeric network swollen with an IL or ILs mixture[60] and have tunable characteristics and structures that enable wide utility in polymer electrolytes,[61] transistors,[62] actuators,[63] and low-voltage, flexible electrochemiluminescent (ECL) device.[64] In general, based on the forces involved in the building up of networks, two main classes of ion gels can be distinguished. One is chemical ion gels, formed by covalent crosslinking IL-philic polymers. Previously, we developed a series of chemical ion gels by *in situ* polymerization of vinyl monomers in ILs.[61] The other is physical ion gels, formed by block copolymers[65,66] or polymer chains are held together by non-covalent bonding interaction such as IL-phobic,[67,68] hydrogen bonding,[69,70] stereocomplex.[71]

Reversible physical ion gels from triblock copolymers are considerable interesting, as they can exhibit a reversible sol-gel transition induced by external stimulus such as temperature and light. In addition, gel structure and physical properties can be controlled through variation of copolymer concentration, block length and composition. For example, Lodge and coworkers reported a thermoreversible ion gel consisting of poly(*N*-isopropylacrylamide)-*block*-poly(ethylene

oxide)-*block*-poly(*N*-isopropylacrylamide)   (PNIPAm-PEO-PNIPAm)   and   a

hydrophobic IL exhibited high temperature sol-state and low temperature gel-state,

whereby the material can be processed in its liquid state and used in its solid state.[72]

The gelation temperature was further adjusted over the range of 17-48 °C by

incorporating   short   solvophobic   PS   blocks   to   produce   well-defined

PNIPAm-PS-PEO-PS-PNIPAm pentablock copolymers, depending on the PS block

length.[65] Our group developed an ion gel that melts on cooling by dissolving a

poly(benzyl   methacrylate)-*block*-poly(methyl   methacrylate)-*block*-poly(benzyl

methacrylate) (PBnMA-PMMA-PBnMA) triblock copolymer in [C$_2$mim][NTf$_2$],

where PBnMA exhibits LCST phase behavior in [C$_2$mim][NTf$_2$] around 105 °C.[66]

More recently, we developed a thermo-/photo-responsive ion gel by gelation of a

triblock copolymer with IL-selective poly(ethylene glycol) (PEG) as midblock and

thermo-/photo-responsive   random   copolymer   of   AzoMA   and   NIPAm

(P(NIPAm-*r*-AzoMA))   as   both   end   blocks   in   a   hydrophobic   IL,

1-butyl-3-methylimidazolium hexafluorophosphate ([C$_4$mim]PF$_6$).[73] This ion gel

showed   both   thermo-induced   reversible   sol-gel   transition   and   photo-induced

reversible sol-gel transition at suitable temperatures. Furthermore, Photo-healable

material can be realized by utilizing such photo-induced sol-gel transition.[74]

1.5 Healable materials

Healable polymers that can be repaired after being damaged are fascinating because

this characteristic can improve the reliability, functionality, and lifetime of many

products.[75,76] A variety of self-healing polymers have been developed. Healing

agents[77] as well as reversible covalent[78,79] and noncovalent bonds[80,81] with the application of stimuli such as heat[82] and light,[78,81] have been utilized to develop self-healing materials. Photo-healable materials are of great interest, because the use of light as stimulus for healing offers several advantages, such as controlled healing in a non-contact way and locally delivered stimulus only to damaged parts. So far, two main classes of photo-healable polymers have been explored;[75] one is structurally dynamic polymers, which are macromolecules that contain dynamic bonds that allow for reorganization of the molecular architecture upon exposure to photo-irradiation. Dynamic bonds including covalent or noncovalent bonds can undergo reversible breaking and reformation reactions by light illumination, as are seen in cinnamoyl,[83] coumarin,[84,85] and disulfide[86,87] groups. The other is mechanically activated reactive systems,[88,89] which are polymers containing labile functional groups that generate active forms upon mechanical damage of the polymer. These reactive functional groups then react together to form new covalent bonds under UV light irradiation, and thereby repair the damaged parts.

For photo-healable triblock copolymer P(NIPAm-*r*-AzoMA)-*b*-PEO-*b*-P(NIPAm-*r*-AzoMA) ion gel, Photo-healing process involves photo-induced liquefying the materials, because of polymer solubility difference under UV light and visible light irradiation in the IL at certain temperatures. After liquefaction, damaged parts are filled with the liquid, followed by gelation of the damaged parts by visible light irradiation. It is apparent that this photo-healable process is different from the two classes of photo-healable polymers mentioned above,

because this photo-healing process involves neither reversible breaking and reformation reactions of dynamic bonds nor mechanically activated reactive chemistry. This ion gel possesses many advantages such as thermo- and photo-processablility, in addition to photo-healable merits. Unique characteristics of IL such as high thermal and chemical stability, negligible vapor pressure, low-flammability, and high ionic conductivity afford the gels valuable properties. However, the triblock copolymer ion gels include relatively many network defects including loops and dangling chains,[90] which lead to lower mechanical properties, especially lower modulus and higher critical gelation concentration of self-standing gels. It was reported that a triblock copolymer ion gel, where the end block microdomains were chemically cross-linked, significantly improved its toughness.[91] However, a precious property of sol-gel transition was lost. It is of our great interest to develop a new route to obtain ion gels with not only high modulus and fewer network defects, but also preservation of reversible sol-gel transition properties.

1.6 Objective and assumption of this work

The overall objective of this thesis research is to improve mechanical properties and decrease network defects of ion gels by using self-assembly of tetra-arm diblock copolymer in an IL, and meanwhile, elucidate the relationship of morphology of micelles and architecture of block copolymers. Because, in dilute solution, the self-assembly of star polymers in ILs has not been reported yet, thus, it is also interesting to develop and accumulate such knowledge of self-assembly of star polymers in ILs.

In this thesis, we prepared a tetra-arm diblock copolymer, in which IL-philic polymer tetra-PEG as central block and thermo-/photo-responsive polymer P(NIPAm-*r*-AzoMA) as four end blocks. We assume that ion gels from tetra-arm diblock copolymers have higher mechanical properties and smaller network defects. Because this ion gels have four kinds of bridges between two end block microdomains ((i) four end blocks connect four different microdomains; (ii) two end blocks belong to the same microdomain, the other two end blocks associate with two different microdomains; (iii) two end blocks connect the same microdomain, the other two belong to another same microdomain; (iv) one end block belong to a microdomain, the other end blocks connect the same microdomain) (**Figure 1.11a**). Conversely, only one kind of bridge is formed for triblock copolymer ion gels (**Figure 1.11b**). Therefore, the possibility to form bridges for tetra-arm diblock copolymer ion gels is apparently higher than that for triblock copolymer ion gels. In principle, tetra-arm diblock copolymer ion gels should have higher mechanical properties and smaller network defects than triblock copolymer ion gels.

(a) $A(B)_4$

(i)

(ii)

(iii)

(iv)

(b) $A(B)_2$
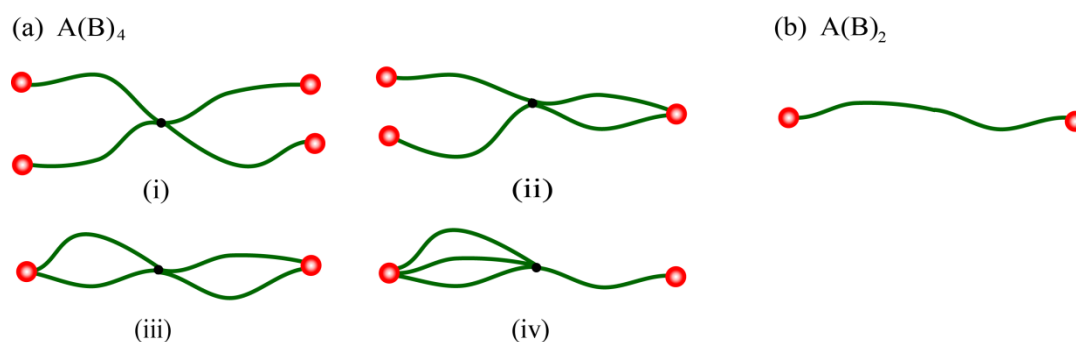
Figure 1.11. Schematic illustration of bridges between block domains for $A(B)_4$ ion gel (a) and $A(B)_2$ ion gel (b).

1.7 Thesis overview

This dissertation is outlined as follows:

Chapter 2 describes the experimental details of the polymers synthesis and characterization, and the experimental techniques, including size exclusion chromatography, dynamic light scattering, rheology and tensile test.

Chapter 3 investigates the DLS consequences of 1 wt% triblock copolymer and tetra-arm diblock copolymer in $[C_4mim]PF_6$. Thermo-induced self-assembly of both polymers solutions was studied under dark conditions and UV light irradiation. Photo-induced self-assembly of both polymers solutions also be investigated.

Chapter 4 demonstrates rheological properties of concentrated solutions of both polymers. Gelation properties and mechanical properties comparison between both ion gels were discussed, thermo-/photo-induced sol-gel transition also be studied. It is found that photo-induced sol-gel transition was completely reversible. Photo-healable material can be realized by using this transition. Photo-healing property and healing efficiency also be shown in this chapter.

Chapter 5 summarizes the research presented in this thesis and recommends directions for future work.

1.8 References

1 Seddon, K. R. *Nature Materials* **2003**, *2*, 363-365.

2 Greaves, T. L.; Drummond, C. J. *Chem. Rev.* **2008**, *108*, 206-237.

3 Walden, P. *Bull. Acad. Imp. Sci.* (St. Petersburg) **1914**, 405.

4 Wilkes, J. S.; Levisky, J. A.; R. Wilson, A.; Hussey, C. L. *Inorg. Chem.* **1982**, *21*, 1263-1264.

5 Wilkes, J. S.; Zaworotko, M. J. *J. Chem. Soc., Chem. Commun.* **1992**, *13*, 965-967.

6 Rogers, R. D.; Seddon, K. R. *Science* **2003**, *302*, 792-793.

7 Welton, T. *Chem. Rev.* **1999**, *99*, 2071-2084.

8 Kuwabata, S.; Tsuda, T.; Torimoto, T. *J. Phys. Chem. Lett.* **2010**, *1*, 3177-3188.

9 Maddikeri, R. R.; Colak, S.; Gido, S. P.; Tew, G. N. *Biomacromolecules* **2011**, *12*, 3412-3417.

10 Zhong, S.; Pochan, D. J. *Polym. Rev.* **2010**, *50*, 287-320.

11 Kim, H.-S.; Choi, G.-Y.; Moon, S.-I.; Kim, S.-P. *Journal of Applied Electrochemistry* **2003**, *33*, 491-496.

12 (a) Lewandowski, A.; Świderska, A. *Solid State Ionics* **2003**, *161*, 243. (b) Isshiki, Y.; Nakamura, M.; Tabata, S.; Dokko, K.; Watanabe, M. *Polym. Adv. Tech.* **2011**, *22*, 1254.

13 (a) Lee, S.-Y.; Yasuda, T.; Watanabe, M. *J. Power Sources* **2010**, *195*, 5909. (b) Lee, S.-Y.; Ogawa, A.; Kanno, M.; Nakamoto, H.; Yasuda, T.; Watanabe, M. *J. Am. Chem. Soc.* **2010**, *132*, 9764.

14 Shobukawa, H.; Tokuda, H.; Susan, M.; Watanabe, M. *Electrochim. Acta* **2005**, *50*, 3872.

15 Armand, M.; Endres, F.; MarFarlane, D. R.; Ohno, H.; Scrosati, B. *Nat. Mater.*

2009, *8*, 621-629.

16 Tokuda, H.; Ishii, K.; Susan, M. A. B. H.; Tsuzuki, S.; Hayamizu, K.; Watanabe, M. *J. Phys. Chem. B* **2006**, *110*, 2833-2839.

17 Tokuda, H.; Hayamizu, K.; Ishii, K.; Susan, M. A. B. H.; Watanabe, M. *J. Phys. Chem. B* **2004**, *108*, 16593-16600.

18 Tokuda, H.; Hayamizu, K.; Ishii, K.; Susan, M. A. B. H.; Watanabe, M. *J. Phys. Chem. B* **2005**, *109*, 6103-6110.

19 Swatloski, R. P.; Spear, S. K.; Holbrey, J. D.; Rogers, R. D. *J. Am. Chem. Soc.* **2002**, *124*, 4974-4975.

20 Phillips, D. M.; Drummy, L. F.; Conrady, D. G.; Fox, D. M.; Naik, R. R.; Stone, M. O.; Trulove, P. C.; De Long, H. C.; Mantz, R. A. *J. Am. Chem. Soc.* **2004**, *126*, 14350.

21 Hameed, N.; Guo, Q. *Carbohydr. Polym.* **2009**, *78*, 999.

22 Xie, H.; Li, S.; Zhang, S. *Green Chem.* **2005**, *7*, 606.

23 Qin, Y.; Lu, X.; Sun, N.; Rogers, R. D. *Green Chem.* **2010**, *12*, 968.

24 Hallett, J. P.; Welton, T. *Chem. Rev.* **2011**, *111*, 3508-3576.

25 Noda, A.; Watanabe, M. *Electrochimica Acta* **2000**, *45*, 1265-1270.

26 Dupont, J.; de Souza, R. F.; Suarez, P. A. Z. *Chem. Rev.* **2002**, *102*, 3667-3692.

27 Han, X.; Armstrong, D. W. *Acc. Chem. Res.* **2007**, *40*, 1079-1086.

28 Holbrey, J. D.; Reichert, W. M.; Nieuwenhuyzen, M.; Sheppard, O.; Hardacre, C.; Rogers, R. D. *Chem. Commun.* **2003**, *39*, 476.

29 Lee, H.-N., Lodge, T. P. *J. Phys. Chem. B* **2011**, *115*, 1971-1977.

30 Lee, H.-N.; Lodge, T. P. *J. Phys. Chem. Lett.* **2010**, *1*, 1962-1966.

31 Tsuda, R.; Kodama, K.; Ueki, T.; Kokubo, H.; Imabayashi, S.; Watanabe, M.

Chem. Commun. **2008**, *44*, 4939-4941.

32 Ueki, T.; Watanabe, M. *Chem. Lett.* **2006**, *35*, 964-965.

33 Ueki, T.; Yamaguchi, A.; Ito, N.; Kodama, K.; Sakamoto, J.; Ueno, K.; Kokubo, H.; Watanabe, M. *Langmuir* **2009**, *25*, 8845-8848.

34 Ueki, T.; Nakamura, Y.; Yamaguchi, A.; Niitsuma, K.; Lodge, T. P.; Watanabe, M. *Macromolecules* **2011**, *44*, 6908-6914.

35 Ueki, T.; Nakamura, Y.; Lodge, T. P.; Watanabe, M. *Macromolecules* **2012**, *45*, 7566-7573.

36 Schacher, F. H.; Rupar, P. A.; Manners, Ian. *Angew. Chem. Int. Ed.* **2012**, *51*, 7898-7921.

37 Bucknall, D. G.; Anderson, H. L.; *Science* **2003**, *302*, 1904-1905.

38 Meuler, A. J.; Hillmyer, M. A.; Bate, F. S. *Macromolecules* **2009**, *42*, 7221.

39 Geng, Y.; Dalhaimer, P.; Cai, S.; Tsai, R.; Tewari, M.; Minko, T.; Discher, D. E. *Nat. Nanotechnol.* **2007**, *2*, 249-255.

40 Rodionov, V.; Gao, H.; Scroggins, S.; Unruh, D. A.; Avestro, A.-J.; Fréchet, J. M. J. *J. Am. Chem. Soc.* **2010**, *132*, 2570-2572.

41 Jones, B. H.; Lodge, T. P. *J. Am. Chem. Soc.* **2009**, *131*, 1676.

42 Kang, Y.; Walish, J. J.; Gorishnyy, T.; Thomas, E. L. *Nat. Mater.* **2007**, *6*, 957-960.

43 Barrett, C. J.; Mamiya, J. I.; Yager, K. G.; Ikeda, T. *Soft Matter* **2007**, *3*, 1249-1261.

44 Tsarevsky, N. V.; Matyjaszewski, K. *Chem. Rev.* **2007**, *107*, 2270.

45 Chiefari, J.; Chong, Y. K.; Ercole, F.; Krstina, J.; Jeffery, J.; Le, T. P. T.; Mayadunne, R. T. A.; Meijs, G. F.; Moad, C. L.; Moad, G.; Rizzardo, E.; Thang, S. H.

Macromolecules **1998**, *31*, 5559.

46 Benoit, D.; Chaplinski, V.; Braslau, R.; Hawker, C. J. *J. Am. Chem. Soc.* **1999**, *121*, 3904.

47 He, Y.; Li, Z.; Simone, P.; Lodge, T. P. *J. Am. Chem. Soc* **2006**, *128*, 2745-2750.

48 Bai, Z.; He, Y.; Lodge, T. P. *Langmuir* **2008**, *24*, 5284-5290.

49 He, Y. Lodge, T. P. *J. Am. Chem. Soc* **2006**, *128*, 12666-12667.

50 Tamura, S.; Ueki, T.; Ueno, K.; Kodama, K.; Watanabe, M. *Macromolecules* **2009**, *42*, 6239.

51 Lee, H.-N.; Lodge, T. P. *J. Phys. Chem. B* **2011**, *115*, 1971-1977.

52 Hoarfrost, M. L.; Lodge, T. P. *Macromolecules* **2014**, *47*, 455-1461.

53 Ueki, T.; Watanabe, M.; Lodge, T. P. *Macromolecules* **2009**, *42*, 1315-1320.

54 Lee, H.-N.; Bai, Z.; Newell, N.; Lodge, T. P. *Macromolecules* **2010**, *43*, 9522-9528.

55 Zhuang, J.; Gordon, M. R.; Ventura, J.; Li, L. Thayumanavan, S. *Chem. Soc. Rev.* **2013**, *42*, 7421-7435.

56 Simone, P. M.; Lodge, T. P. *Macromolecules* **2008**, *41*, 1753-1759.

57 Simone, P. M.; Lodge, T. P. *Acs Applied Materials & Interfaces* **2009**, *12*, 2812-2820.

58 Hoarfrost, M. L.; Segalman, R. A. *Macromolecules* **2011**, *44*, 5281-5288.

59 Noro, A.; Tomita, Y.; Shinohara, Y.; Sageshima, Y.; Walish, J. J.; Matsushita, Y.; Thomas, E. L. *Macromolecules* **2014**, *47*, 4103-4109.

60 Lodge, T. P. *Science* **2008**, *321*, 50-51.

61 Susan, M. A. B. H.; Kaneko, T.; Noda, A.; Watanabe, M. *J. Am. Chem. Soc.* **2005**, *127*, 4976-4983.

62 Cho, J.-H.; Lee, J.; Xia, Y.; Kim, B.-S.; He, Y.; Renn, M. J.; Lodge, T. P.; Frisbie, C. D. *Nat. Mater.* **2008**, *7*, 900-906.

63 Imaizumi, S.; Kokubo, H.; Watanabe, M. *Macromolecules* **2012**, *45*, 401-409.

64 Moon, H.; Lodge, T. P.; Frisbie, C. D. *J. Am. Chem. Soc.* **2014**, *136*, 3705-3712.

65 He, Y.; Lodge, T. P. *Macromolecules* **2008**, *41*, 167-174.

66 Kitazawa, Y.; Ueki, T.; Niitsuma, K.; Imaizumi, S.; Lodge, T. P.; Watanabe, M. *Soft Matter* **2012**, *8*, 8067-8074.

67 Singh, B.; Sekhon, S. S. *Chem. Phys. Lett.* **2005**, *414*, 34-39.

68 Singh, B.; Sekhon, S. S. *J. Phys. Chem. B* **2005**, *109*, 16539-16543.

69 Noro, A.; Matsushita, Y.; T. P. Lodge, *Macromolecules* **2008**, *41*, 5839-5844.

70 Noro, A.; Matsushita, Y.; Lodge, T. P. *Macromolecules* **2009**, *42*, 5802-5810.

71 Kawauchi, T.; Kumaki, J.; Okoshi, K.; Yashima, E. *Macromolecules* **2005**, *38*, 9155-9160.

72 He, Y.; Lodge, T. P. *Chem. Commun.* **2007**, *43*, 2732-2734.

73 Ueki, T.; Nakamura, Y.; Usui, R.; Kitazawa, Y.; So, S.; Lodge, T. P.; Watanabe, M. *Angew. Chem. Int. Ed.* **2015**, *54*, 3018-3022.

74 Ueki, T.; Usui, R; Kitazawa, Y.; Lodge, T. P.; Watanabe, M. *Macromolecules* **2015**, *48*, 5928-5933.

75 Fiore, G. L.; Rowan, S. J.; Weder, C. *Chem. Soc. Rev.* **2013**, *42*, 7278-7288.

76 Habault, D.; Zhang, H.; Zhao, Y. *Chem. Soc. Rev.* **2013**, *42*, 7244-7256.

77 White, S. R.; Sottos, N. R.; Geubelle, P. H.; Moore, J. S.; Kessler, M. R.; Sriram, S. R.; Brown, E. N.; Viswanathan, S. *Nature*, **2001**, *409*, 794-797.

78 Froimowicz, P.; Frey, H.; Landfester, K.; *Macromol. Rapid Commun.* **2011**, *32*, 468-473.

79 Capelot, M.; Montarnal, D.; Tournilhac, F.; Leibler, L. *J. Am. Chem. Soc.* **2012**, *134*, 7664-7667.

80 Chen, Y.; Kushner, A. M.; Williams, G. A.; Guan, Z. *Nat. Chem.* **2012**, *4*, 467-472.

81 Burnworth, M.; Tang, L.; Kumpfer, J. R.; Duncan, A. J.; Beyer, F. L.; Fiore, G. L.; Rowan, S. J.; Weder, C. *Nature* **2011**, *472*, 334-337.

82 Chen, X.; Dam, M. A.; Ono, K.; Mal, A.; Shen, H.; Nutt, S. R.; Sheran, K.; Wudl, F. *Science* **2002**, *295*, 1698-1702.

83 Chung, C.-M.; Roh, Y.-S.; Cho, S.-Y.; Kim, J.-G. *Chem. Mater.* **2004**, *16*, 3982-3984.

84 Ling, J.; Rong, M. Z.; Zhang, M. Q. *J. Mater. Chem.* **2011**, *21*, 18373-18380.

85 Ling, J.; Rong, M. Z.; Zhang, M. Q. *Polymer* **2012**, *53*, 2691-2698.

86 Otsuka, H.; Nagano, S.; Kobashi, Y.; Maeda, T.; Takahara, A. *Chem. Commun.* **2010**, *46*, 1150-1152.

87 Fairbanks, B. D.; Singh, S. P.; Bowman, C. N.; Anseth, K. S. *Macromolecules* **2011**, *44*, 2444-2450.

88 Ghosh, B.; Urban, M. W. *Science* **2009**, *323*, 1458-1460.

89 Gosh, B.; Chellappan, K. V.; Urban, M. W. *J. Mater. Chem.* **2011**, *21*, 14473-14486.

90 Kirkland, S. E.; Hensarling, R. M.; McConaughy, S. D.; Guo, Y.; Jarrett, W. L.; McCormick, C. L. *Biomacromolecules* **2008**, *9*, 481-486.

91 Gu, Y.; Zhang, S.; Martinetti, L.; Lee, K.-H.; McIntosh, L. D.; Frisbie, C. D.; Lodge, T. P. *J. Am. Chem. Soc.* **2013**, *135*, 9652-9655.

Chapter 2 Materials synthesis and characterization

2.1 Raw materials.

Tetra-PEG (M_n = 40,000, average molecular weight of each arm = 10,000; M_w/M_n = 1.05) was generously provided by the NOF Corporation. PEG (M_n = 20,000; M_w/M_n = 1.35) was purchased from Sigma-Aldrich. 1,4-Dioxane, dehydrated dichloromethane, 2,2′-Azobis (isobutyronitrile) (AIBN) and oxalyl chloride were purchased from Wako Chemicals. NIPAm was generously provided by the Kojin Corporation and purified by recrystallization (two times) using a toluene/hexane (1:10 by weight) mixed solvent. AIBN was recrystallized from methanol prior to use. Tetra-PEG and PEG were dried by azeotropic distillation using toluene to remove residual water. All other chemical reagents were used as received. [C$_4$mim]PF$_6$,[1] S-1-dodecyl-S′-(α,α′-dimethyl-α″-acetic acid) trithiocarbonate (CTA),[2] and AzoMA[3] were synthesized and characterized according to the procedures found in the literature. The water content of the [C$_4$mim]PF$_6$ was determined by a Karl Fischer titration and was less than 10 ppm. The bromide content of aqueous phases in contact with the [C$_4$mim]PF$_6$ could not be detected by the addition of an AgNO$_3$ aqueous solution. This suggests that the bromide content of the [C$_4$mim]PF$_6$ remained below the solubility limit of AgBr in water (0.2 mg L^{-1}).

2.2 Polymers synthesis

2.2.1 Synthesis of [PEG-*b*-P(AzoMA-*r*-NIPAm)]$_4$ tetra-arm diblock copolymer.

The tetra-arm diblock copolymer (A(B)$_4$) was synthesized according to the procedure shown in **Scheme 2.1**. The first step was to prepare the tetra-PEG-CTA

macro-chain-transfer agent. Tetra-PEG (6.64 g, 0.166 mmol) and dichloromethane (50 mL) were mixed in a round-bottom flask until a transparent solution was obtained. Oxalyl chloride (0.44 mL, 5.1 mmol), CTA (0.620 g, 1.70 mmol) and dehydrated dichloromethane (10 mL) were mixed in another round-bottom flask under an argon atmosphere and stirred at room temperature until gas evolution stopped (~2 h). Excess reagents were then removed under vacuum, and the residue was re-dissolved in dehydrated dichloromethane (12 mL). This solution was then added into the tetra-PEG solution. The reaction was allowed to stir for 24 h at room temperature, after which the contents were reprecipitated 3 times by pouring the tetra-PEG-CTA solution in tetrahydrofuran (THF) (as a good solvent) into cold diethyl ether (as a poor solvent). The precipitate was then dried under vacuum at room temperature overnight to yield tetra-PEG-CTA as a light yellow powder (6.33 g, 90%).

The second step was RAFT copolymerization of NIPAm and AzoMA from the end of the obtained tetra-PEG-CTA. Tetra-PEG-CTA (1.00g, 0.0242 mmol), AzoMA (1.36 g, 5.11 mmol), NIPAm (16.0 g, 0.142 mol) ([AzoMA]/[NIPAm] = 3.5/96.5), and 1,4-dioxane (100 mL) were placed into a round-bottom flask and degassed by purging argon for 30 min at 45 °C. Special attention was given to avoid crystallization of the NIPAm monomer during the bubbling process. AIBN (5.0 mg, 0.030 mmol) was separately dissolved in 1,4-dioxane (5.0 mL) in a separate round-bottom flask and deaerated by purging argon for 30 min at room temperature. The AIBN solution (3.3 mL, 0.020 mmol) was then added to the monomer solution. RAFT polymerization was carried out at 65 °C for 98 h. The reaction mixture was evaporated and purified

by reprecipitation three times from acetone (as a good solvent) to cold diethyl ether (as a poor solvent). The precipitate was collected and dissolved in ethanol at 40 °C, the solution was stored in refrigerator until phase separation. Then the solid phase was collected and purified by reprecipitation one time from acetone (as a good solvent) to cold diethyl ether (as a poor solvent). The precipitate was then dried overnight under vacuum at 40 °C to yield [PEG-*b*-P(AzoMA-*r*-NIPAm)-CTA]$_4$ as a yellow powder (2.10 g, 11%).

Finally, the dodecyl trithiocarbonate residue attached to end blocks of the polymer ([PEG-*b*-P(AzoMA-*r*-NIPAm)-CTA]$_4$) was removed according to the following procedure. [PEG-*b*-P(AzoMA-*r*-NIPAm)-CTA]$_4$ (1.00 g, 0.0107 mmol) and AIBN (0.212 g, 1.29 mmol) were dissolved in 1,4-dioxane (25 mL). The solution was degassed by purging argon for 30 min at room temperature. The cleavage reaction was carried out at 80 °C for 12 h under argon atmosphere. The reaction mixture was evaporated and purified by reprecipitation three times from acetone (as a good solvent) to cold diethyl ether (as a poor solvent). The precipitate was then dried overnight under vacuum at 40 °C to yield [PEG-*b*-P(AzoMA-*r*-NIPAm)]$_4$ as a yellow powder (0.870 g, 87%).
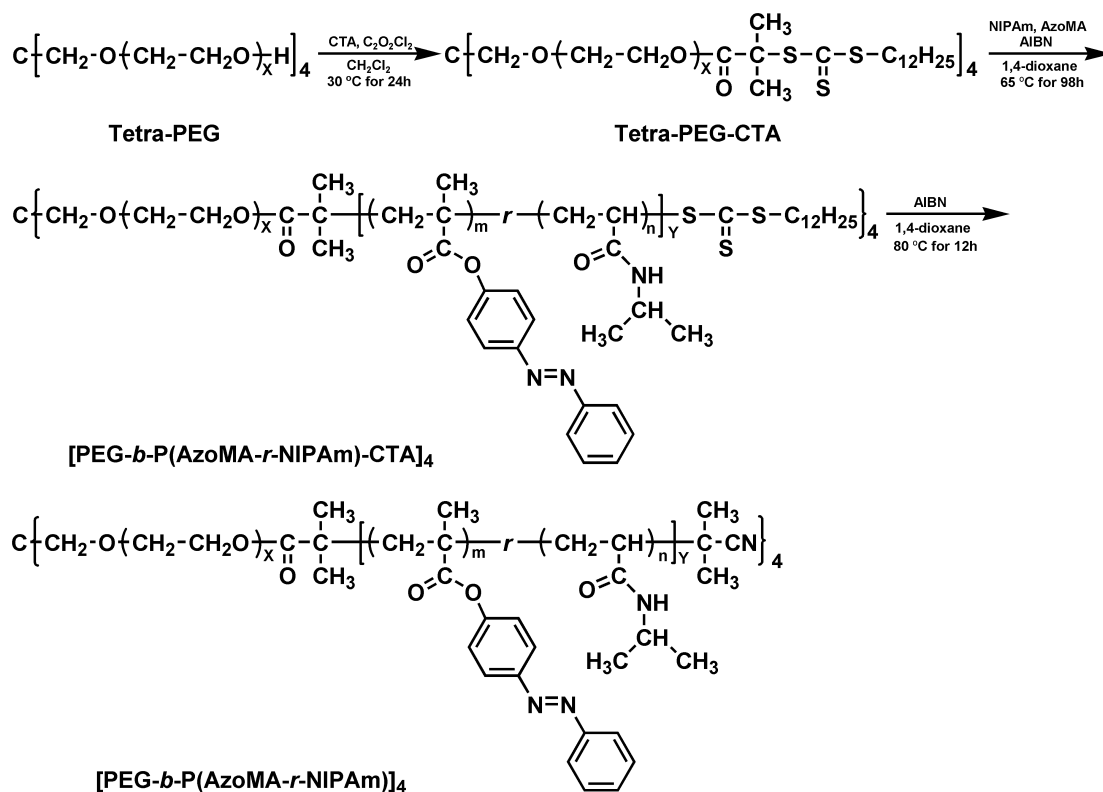
Scheme 2.1. Synthetic procedure for the tetra-arm diblock copolymer.

Tetra-PEG → Tetra-PEG-CTA

[PEG-*b*-P(AzoMA-*r*-NIPAm)-CTA]₄

[PEG-*b*-P(AzoMA-*r*-NIPAm)]₄

2.2.2 Synthesis of P(AzoMA-*r*-NIPAm)-*b*-PEG-*b*-P(AzoMA-*r*-NIPAm) triblock copolymer.

The triblock copolymer (A(B)₂) was prepared according to the procedure shown in **Scheme 2.2**. First step was preparation of PEG-CTA macro-chain transfer agent, the procedure was similar to that of tetra-PEG-CTA, just use linear PEG instead of tetra-PEG. Next step is Synthesis of P(AzoMA-*r*-NIPAm)-*b*-PEG-*b*-P(AzoMA-*r*-NIPAm). PEG-CTA (1.00 g, 0.05 mmol), AzoMA (1.96 g, 7.37 mmol), NIPAm (20.0 g, 177 mmol) ([AzoMA]/[NIPAm] = 4.0/96.0 by mol%), and 1,4-dioxane (120 mL) were mixed in a round-bottom flask and degassed by purging argon for 30 min at 45 °C to avoid crystallization of NIPAm monomer during bubbling process. AIBN (5 mg, 0.0305 mmol) and 1,4-dioxane (5

mL) were separately placed in another round-bottom flask and purged with argon for 30 min at room temperature. The AIBN solution (3.0 mL, 0.0183 mmol) was then added to the monomer solution. RAFT polymerization was conducted at 65 °C for 72 h. The reaction mixtures were evaporated and purified by reprecipitation three times from acetone as a good solvent and cold diethyl ether as a poor solvent. The precipitate was then dried overnight under vacuum at 40 °C to yield triblock copolymer having the dodecyl trithiocarbonate residue derived from the CTAs attached to the polymer termini as a yellow powder (2.0 g, 9.1%).

Finally, the dodecyl trithiocarbonate residue were removed according to the following procedure: the triblock copolymer (1.0 g, 0.0238 mmol) and AIBN (0.117 g, 0.714 mmol) were dissolved in 1,4-dioxane (15 mL), and degassed by purging with argon for 30 min at room temperature. The cleavage reaction was carried out at 80 °C for 12 h under argon atmosphere. The reaction mixture was evaporated and purified by reprecipitation three times from acetone as a good solvent and cold diethyl ether as a poor solvent. The precipitate was then dried overnight under vacuum at 40 °C to yield P(AzoMA-*r*-NIPAm)-*b*-PEG-*b*-P(AzoMA-*r*-NIPAm) as a yellow powder (0.80 g, 80%).

Scheme 2.2. Synthetic procedure for the triblock copolymer.

2.3 Characterization of both polymers

The products of each reaction step in **Scheme 2.1 and Scheme 2.2** were identified by ^{1}H NMR (**Figures 2.1, 2.2,** and **2.3**). The end group conversion ratio of tetra-PEG-CTA or PEG-CTA was calculated from the ^{1}H NMR spectrum (**Figure 2.1**) by comparing integrated signal intensities of the methylene protons in the tetra-PEG main chain (c) with that of the methyl protons in CTA (a) and was found to be unity. The peak of methyl protons in CTA disappeared completely in **Figure 2.3** by comparing **Figure 2.1, 2.2** and **2.3**, indicating the dodecyl trithiocarbonate residue attached to end blocks of both polymers were removed completely. The number-average molecular weight (M_n) of A(B)$_4$ and A(B)$_2$ triblock copolymer were calculated from the ^{1}H NMR spectra (**Figure 2.3**) by comparing the integrated signal intensities of the tetra-PEG or PEG main chain ((f) 3.6 ppm) with that of the end blocks ((c) 4.0 ppm from NIPAm; (d) 7.9 ppm from AzoMA). The AzoMA composition was calculated from the ratio of integrated signal intensities between NIPAm and AzoMA, which showed that 6.1 mol% and 9.0 mol% for A(B)$_4$ and

A(B)$_2$ copolymer, respectively.

Figure 2.1. ^{1}H NMR spectra of tetra-PEG-CTA (upper) PEG-CTA (bottom) in CDCl$_3$.

Figure 2.2. ^{1}H NMR spectra of [PEG-*b*-P(AzoMA-*r*-NIPAm-CTA)]$_4$ (upper) triblock copolymer CTA (bottom) in CDCl$_3$.
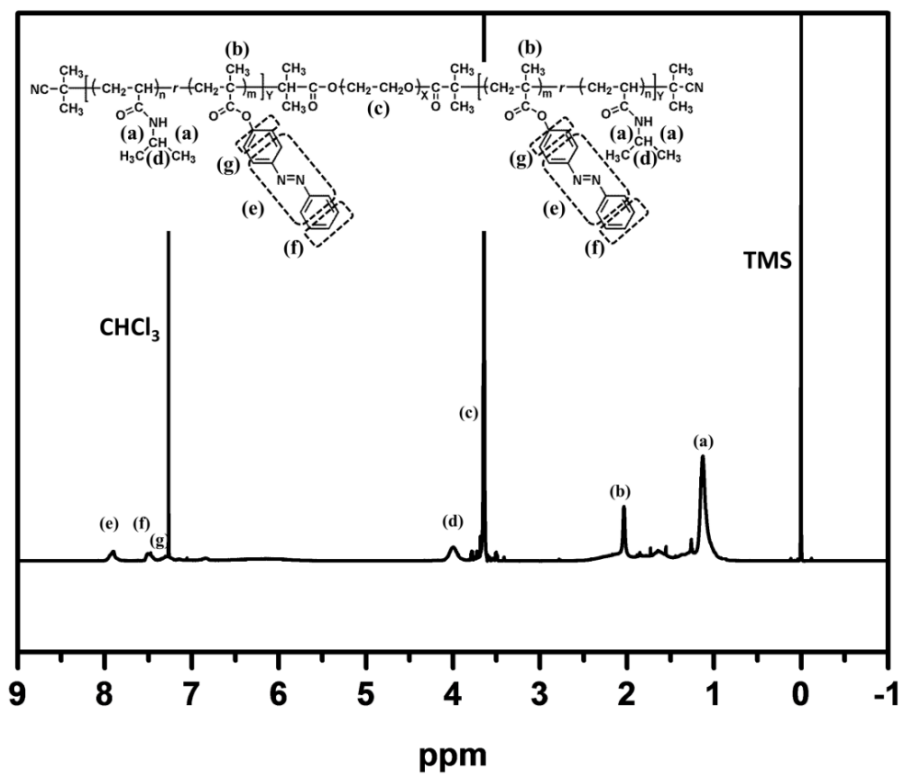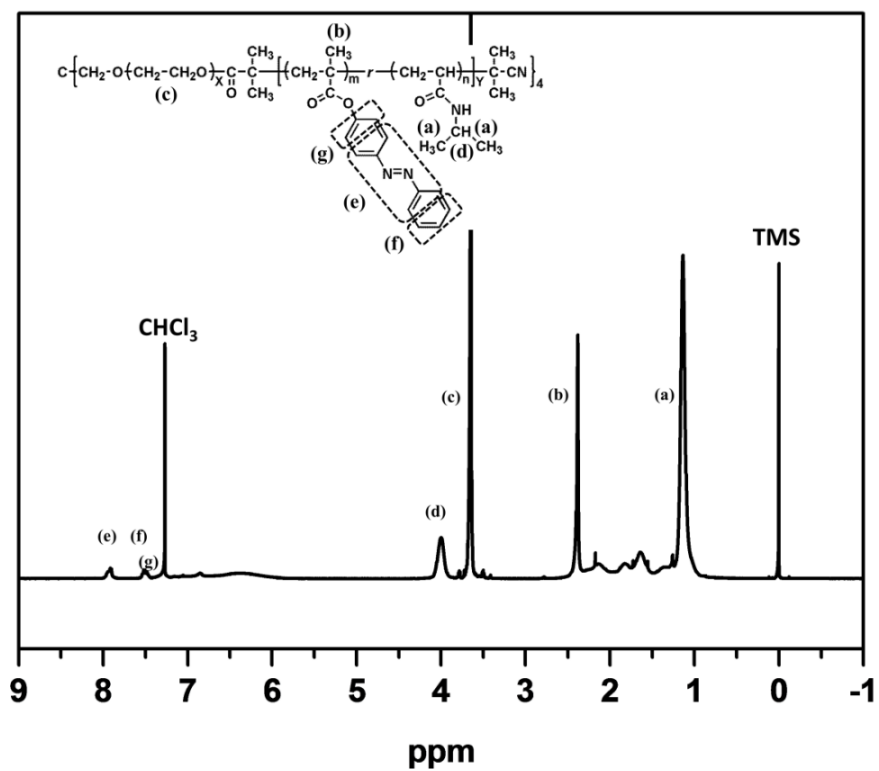
Figure 2.3. ^{1}H NMR spectra of A(B)$_4$ (upper) and A(B)$_2$ (bottom) copolymers

Changes in the GPC traces with each reaction step of both polymers are shown in **Figure 2.4** and **2.5**. In the GPC trace of tetra-PEG, a satellite peak was observed at a longer elution time than that of the main peak, which corresponded to PEG having M_n = 10 kDa, one fourth of M_n of tetra-PEG, which appeared to be originated from trace amount of water in the preparation system. This satellite peak still persisted in the GPC trace of tetra-PEG-CTA. However, for tetra-arm diblock copolymer, before purification of tetra-arm diblock copolymer ([PEG-*b*-P(AzoMA-*b*-NIPAm)-CTA]$_4$), the block copolymer has higher PDI (1.64). After purification, the PDI of block copolymer decreased to 1.35, which indicates lower molecular weight block copolymers starting from the low molecular weight PEG were effectively removed by the fractional precipitation. Thus, the GPC traces of [PEG-*b*-P(AzoMA-*r*-NIPAm)-CTA]$_4$ and [PEG-*b*-P(AzoMA-*r*-NIPAm)]$_4$ were unimodal. For triblock copolymer, the GPC traces of triblock copolymers were also unimodal (**Figure 2.5**). Although polymers generally prepared by living radical polymerization usually have a lower M_w/M_n than 1.2. However, M_w/M_n of A(B)$_4$ and A(B)$_2$ polymers were 1.35 and 1.41, respectively. This is due to the fact that the polymerization is less controlled due to retarding or inhibiting effect of the azobenzene group for radicals.[4] Characterization results of both polymers are summarized in **Table 2.1**. All of the data supported successful preparation of the tetra-arm diblock copolymer A(B)$_4$ and triblock copolymer A(B)$_2$.
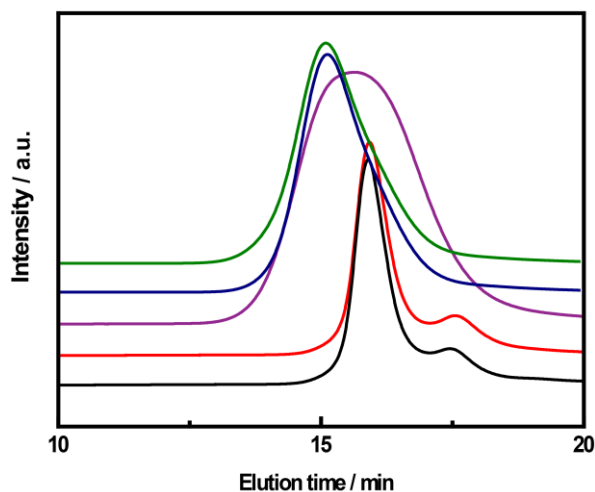
Figure 2.4. GPC traces of tetra-PEG (black line), tetra-PEG-CTA (red line), [PEG-*b*-P(AzoMA-*r*-NIPAm)-CTA]$_4$ before and after fractional precipitation (purple and blue line, respectively) and [PEG-*b*-P(AzoMA-*r*-NIPAm)]$_4$ (green line). DMF was used as the elution solvent at a flow rate of 1.0 ml/min.
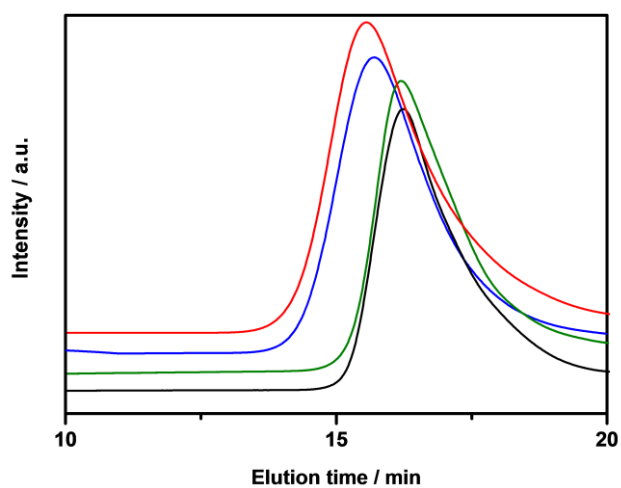
Figure 2.5. GPC traces of PEG (black line), PEG-CTA (green line), triblock copolymer attached to CTA (blue line) and triblock copolymer (red line). DMF was used as the eluent at a flow rate of 1.0 ml/min.

Table 2.1. Characterization results of polymers

Polymers	M_n / kDa [a]	A block M_n / kDa [b]	B block M_n / kDa [a]	M_w/M_n [b]	[AzoMA] / [NIPAm] [a]
A(B)$_2$	42	20	11	1.41	9.0 / 91.0
A(B)$_4$	84	40	11	1.35	6.1 / 93.9

[a] Determined by ^{1}H NMR. [b] Determined by GPC (calibrated with polystyrene standards).

2.4 Preparation of polymer solutions.

A series of polymer solutions were prepared at polymer concentrations of 1, 2, 3, 4, 5, 7, 10, 15 and 20%. For each sample, the polymer was firstly dissolved in THF, followed by the addition of an appropriate amount of [C$_4$mim]PF$_6$. The solution was then stirred at 55 °C for at least 3 h until a transparent solution was obtained and most of THF was volatilized. Residual THF was removed by evaporation at 80 °C under vacuum for 24 h.

2.5 Dynamic light scattering (DLS) measurements.

1 wt% sample solution of A(B)$_2$ or A(B)$_4$ polymers for DLS measurements was passed through 0.20 μm filter to eliminate dust prior to use. Dynamic Light Scattering (DLS) was performed using an Otsuka Electronics DLS-6500 equipped with an ALV correlator and a He-Ne laser with wavelength of 633 nm. Temperatures were controlled to within an accuracy of ±0.1 °C using an index-matching silicon oil bath. Experiments were performed at various temperatures from 50 to 30 °C in a cooling process. The intensity correlation functions $g_2(q, t)$ were recorded at a scattering angle

of 90° at each temperature for 30 s to obtain the relationship between R_h values and temperatures. The intensity correlation function data for photoreversible micellization were collected every 30 s to make the time resolution of each measurement, which is faster than that of the photoinduced micellization process. Data was collected after equilibrating at each temperature for at least 30 min.

For solutions containing monodisperse particles, the electric field correlation function $g_1(q, t)$ displays a single exponential decay,

$$g_1(q,\ t)\ =\ \exp(-\Gamma t)\ =\ \exp(-D_0 q^2 t) \tag{2.1}$$

where t is the time, q is the scattering vector ($q = (4\pi n/\lambda)\sin(\theta/2)$; n is the refractive index of the solutions, λ is the wavelength of the light in vacuum, and θ is the scattering angle), Γ is the decay rate, and D_0 is the mutual diffusion coefficient at infinite dilution. The recorded intensity correlation function $g_2(q, t)$ was converted to $g_1(q, t)$ through the Siegert relation.[5] The hydrodynamic radius, R_h, can be calculated using the solvent viscosity, η, and the Stokes-Einstein equation,

$$R_h\ =\ (k_b T)/6\pi\eta D_0 \tag{2.2}$$

where k_b and T are the Boltzmann constant and absolute temperature, respectively. For solutions with polydisperse (not monomodal) particles, $g_1(q, t)$ can be analyzed by the method of cumulants,[6]

$$g_1(q,\ t)\ =\ A\ \exp(-\Gamma t)(1\ +\ (1/2!)\mu_2 t^2\ -\ (1/3!)\mu_3 t^3) \tag{2.3}$$

where Γ is the mean decay rate and μ_2/Γ^2 represents the width of the distribution. In this study, the apparent hydrodynamic radius, R_h, was calculated using Equation (2.2) by replacing D_0 with $D = \Gamma/q^2$ of the 1 wt% solutions. The distribution of R_h was also

examined by applying the inverse Laplace transformation to $g_1(q, t)$ with the well-established CONTIN program,[7] and by a sum of two exponentials. To estimate R_h, the temperature dependence of the viscosity of $[C_4mim]PF_6$ was calculated using the appropriate Vogel–Tammann–Fulcher (VTF) equation,[8]

$$\eta = 0.36 \ \exp[639/(T - 201)] \tag{2.4}$$

where T (K) is the absolute temperature. The refractive index of $[C_4mim]PF_6$ was calculated using equation,[9]

$$n = 1.49569 - 3.2 \times 10^{-4} \ T + 8.8 \times 10^{-8} \ T^2 \tag{2.5}$$

where T (K) is the absolute temperature. Photoirradiation was carried out using a 500 W high-pressure mercury lamp (Ushio Optical Modulex BA-H500). The wavelength and intensity of the irradiated light (UV light: 366 nm, 8 mW cm^{-2}; visible light: 437 nm, 4 mW cm^{-2}) were adjusted using color filters. Either UV (366 nm) or visible light (437 nm) was irradiated from the upper side of the DLS sample tube (1 cm diameter). A transparent heat-absorbing filter covered the top of the sample tube to avoid the generation of heat from the mercury lamp and contamination by dust.

2.6 Rheology.

Oscillatory shear measurements were conducted on an Anton Paar Physica MCR 301 rheometer using the 25 mm parallel plate geometry. A gap spacing of about 0.2 mm was used for all measurements. The dynamic shear moduli (G' and G'') were examined in the linear viscoelastic regime. For rheology measurements under light illumination, a standard cell for UV measurements (P-PTD200/GL and H-PTD200, Anton Paar) was used under UV (366 nm, 8 mW/cm^2) and visible (437 nm, 4

mW/cm^2) light irradiation. 500 W high-pressure mercury lamp (Ushio Optical Modulex, BA-H50) was used as a light source, and the wavelength of irradiated light were adjusted by using color filters. A heat-absorbing filter was also used to cut the heat generated by the mercury lamp.

2.7 Photo-healing experiment.

A dumb-bell sample of A(B)$_4$ or A(B)$_2$ ion gel (16 mm×4 mm×1 mm) was cut into two pieces at the middle, and then fresh surfaces of the two pieces were touched together and placed on a hot stage of 38 ℃ . A piece of silicone rubber (3 mm×3 mm×1 mm) was placed on either side of the damaged part of the dumb-bell sample to prevent sample from flowing and from shape change during photo-healing process. A mask with a small window (5 mm×3 mm) in the center was covered on the sample to avoid irradiating remaining part without damage. The damaged part of the sample was irradiated by UV light through the window of the mask.

2.8 Tensile tests.

The tensile test specimens were made by adding block copolymer/[C$_4$mim]PF$_6$ sols to a dumb-bell shaped mold at 80 °C, and then decrease temperature to room temperature to obtain dumb-bell shaped gels (16 mm×4 mm×1 mm). A Shimadzu Electromechanical Tester (EZ-LX) with a data acquisition system was utilized to carry out the tensile tests. The tests were carried out at room temperature at 6 mm/min elongation speed.

2.9 References

1 Tokuda, H.; Hayamizu, K.; Ishii, K.; Susan, M. A. B. H.; Watanabe, M. *J. Phys. Chem. B* **2004**, *108*, 16593-16600.

2 Lai, J. T.; Filla, D.; Shea, R. *Macromolecules* **2002**, *35*, 6754-6756.

3 Yuan, W.; Jiang, G.; Wang, J.; Wang, G.; Song, Y.; Jiang, L. *Macromolecules* **2006**, *39*, 1300-1303.

4 Luo, C.; Zuo, F.; Ding, X.; Zheng, Z.; Cheng, X.; Peng, Y. *J. Appl. Polym. Sci.* **2008**, *4*, 2118-2125.

5 Brown, W., Ed.; *Dynamic Light Scattering: The Method and Some Applications*; Clarendon Press: Oxford, 1993.

6 Koppel, D. E. *J. Chem. Phys.* **1972**, *57*, 4814-4820.

7 Provencher, S. W. *Comput. Phys. Commun*. **1982**, *27*, 213-227.

8 Lai, J. T.; Filla, D.; Shea, R. *Macromolecules* **2002**, *35*, 6754-6756.

9 Pereiro, A. B.; Legido, J. L.; Rodríguez, A. *J. Chem. Thermodynamics* **2007**, *39*, 1168-1175.

Chapter 3 Self-assembly of A(B)$_4$ and A(B)$_2$ in dilute solution

Self-assembly of tetra-arm diblock copolymer in aqueous media or organic solvents has been developed. [1,2] A variety of morphologies have been obtained by self-assembly of tetra-arm diblock copolymers, such as core-shell spherical micelles, [3,4] cylindrical micelles[3] and clusters[5]. However, the self-assembly of tetra-arm diblock copolymer in IL has not been reported yet. And how block copolymer architecture affects the aggregation states is also of great interest. We need to accumulate such knowledge because the information on self-assembly of block copolymer in ILs is rather poor, compared with that in water and organic solvents. Therefore, it becomes necessary and important to investigate the relationship between polymer structure and aggregate states.

In this chapter, we describe thermo- and photoinduced self-assembly changes of a tetra-arm diblock copolymer (A(B)$_4$) and triblock copolymer (A(B)$_2$) in [C$_4$mim]PF$_6$. We first describes the thermosensitive self-assembly of both polymers in [C$_4$mim]PF$_6$. Then it describes the reversible photo-induced unimer/micelle transitions by alternating irradiation by UV and visible light at a suitable temperature.

3.1 Thermosensitivity of the A(B)$_4$ and A(B)$_2$ polymers in [C$_4$mim]PF$_6$.

Figure 3.1 and **3**.**2** show the normalized scattering intensity and hydrodynamic radius of 1 wt% tetra-arm diblock copolymer (A(B)$_4$) solution and 1 wt% triblock copolymer (A(B)$_2$) solution, respectively, in [C$_4$mim]PF$_6$ with or without UV light irradiation at a scattering angle of 90°. The normalized scattering intensities were

defined as the intensity at each temperature divided by that at 50 °C. Under dark conditions, the isomerization state of the azobenzene was composed of the *trans*-state (≈100%), whereas under UV light irradiation the *cis*-state (≈80%) dominated[6,7] In the cooling process from 50 °C, the scattered intensity increased with a decrease in temperature of both polymer solutions in the dark and under UV light irradiation (**Figure 3.1a** and **3**.**2a**), due to the UCST nature of the P(AzoMA-*r*-NIPAm) segments. This implies that the tetra-arm diblock copolymers and triblock copolymers aggregates into large size micelles, which scatter the incident light. The aggregation behavior was thermally reversible. For both polymer solutions, the mean hydrodynamic radius (R_h) of the *trans*- and *cis*-form polymer were also determined (**Figure 3.1b** and **3.2b**).
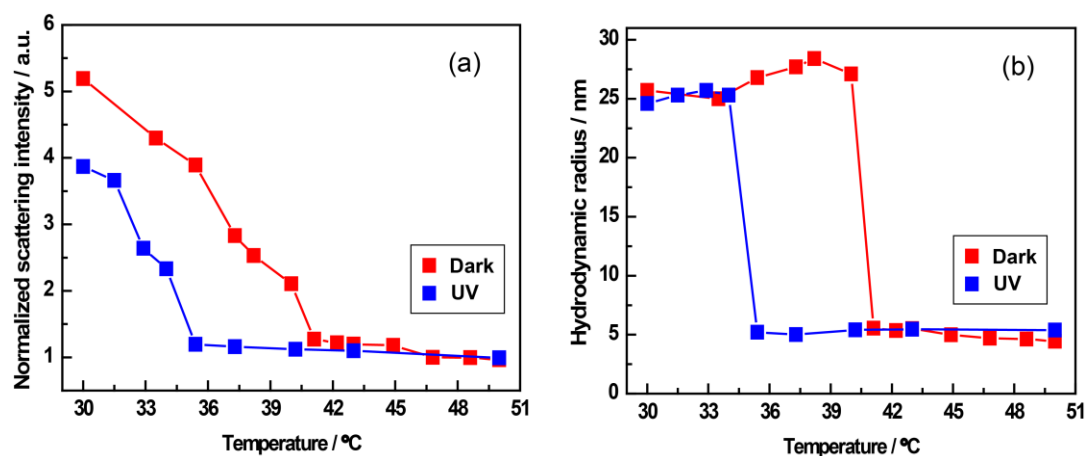
Figure 3.1. (a) Temperature dependence of normalized scattering intensity for A(B)$_4$ (1 wt%) in [C$_4$mim]PF$_6$ under dark conditions (red squares) and with UV light irradiation (blue squares) at a scattering angle of 90°. (b) Temperature dependence of the hydrodynamic radius (R_h) for A(B)$_4$ (1 wt%) in [C$_4$mim]PF$_6$ under dark conditions (red squares) and with UV light irradiation (blue squares).
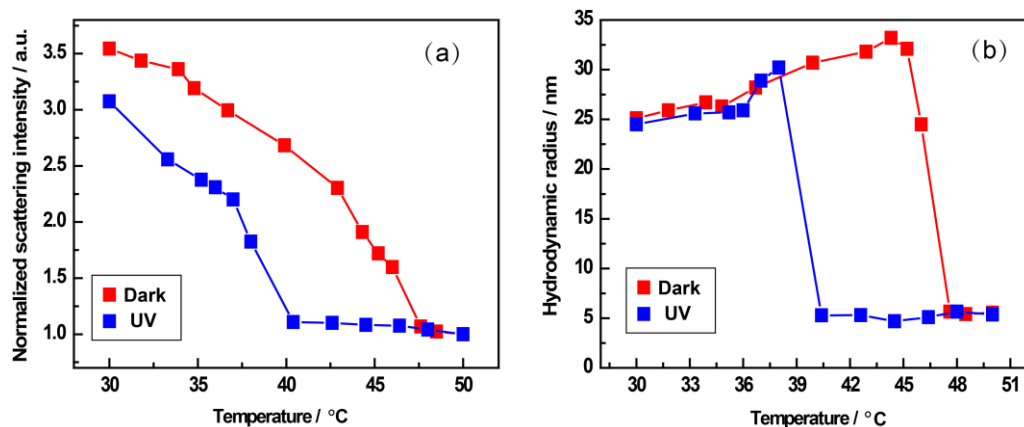
Figure 3.2. (a) Temperature dependence of normalized scattering intensity for A(B)$_2$ (1 wt%) in [C$_4$mim]PF$_6$ under dark conditions (red squares) and with UV light irradiation (blue squares) at a scattering angle of 90°. (b) Temperature dependence of the hydrodynamic radius (R_h) for A(B)$_2$ (1 wt%) in [C$_4$mim]PF$_6$ under dark conditions (red squares) and with UV light irradiation (blue squares).

At higher temperatures than the upper critical micellization temperature (UCMT), the distribution function was bimodal both in the dark and under UV light irradiation (**Figure 3.3**, **3.4** for A(B)$_4$ and **Figure 3.5**, **3.6** for A(B)$_2$). The smaller R_h peak corresponds to the single polymer chains (unimers), whereas the larger R_h peak indicates the existence of aggregates (**Figure 3.3b**, **3.4b** for A(B)$_4$ and **Figure 3.5b**, **3.6b** for A(B)$_2$). The weight fraction of the unimer is calculated to be over 0.999 using a previously reported method,[8] and it was considered that almost all of the scattering in [C$_4$mim]PF$_6$ above the UCMT came from single polymer chains. There are two possible reasons for this small amount of aggregates at higher temperatures. One reason is that these aggregates might arise from solubility differences due to chain-to-chain variations in the comonomer distribution and composition in the

random copolymer block; the other reason is these aggregates may result from the tiny fraction of polymers with very high molecular weight that are reluctant to dissolve. the R_h of the unimer for both polymer solutions is less than 10 nm, consistent with the size of single polymer chains for A(B)$_4$ and A(B)$_2$ with a molecular weight of 84 kDa and 42 kDa, respectively.
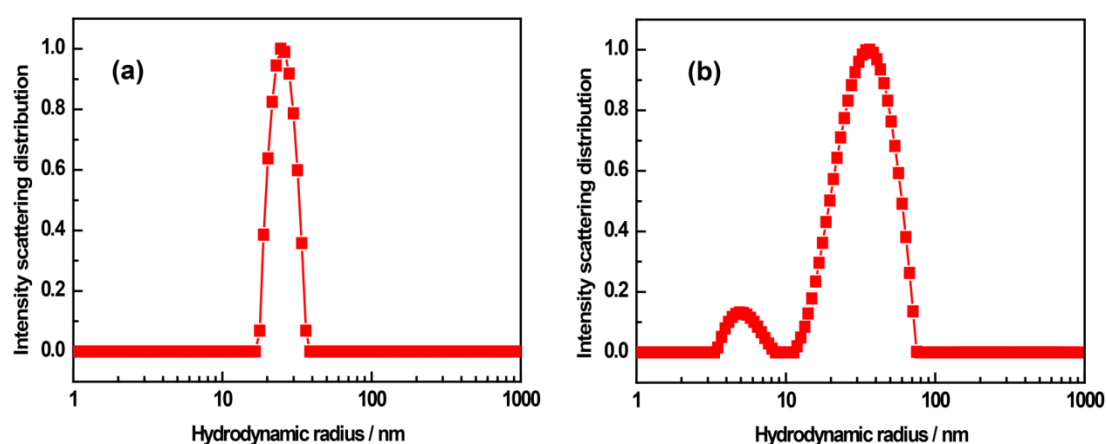
Figure 3.3. CONTIN results for A(B)$_4$ in [C$_4$mim]PF$_6$ (1 wt %) solution at (a) 30 °C and (b) 50 °C under dark conditions.
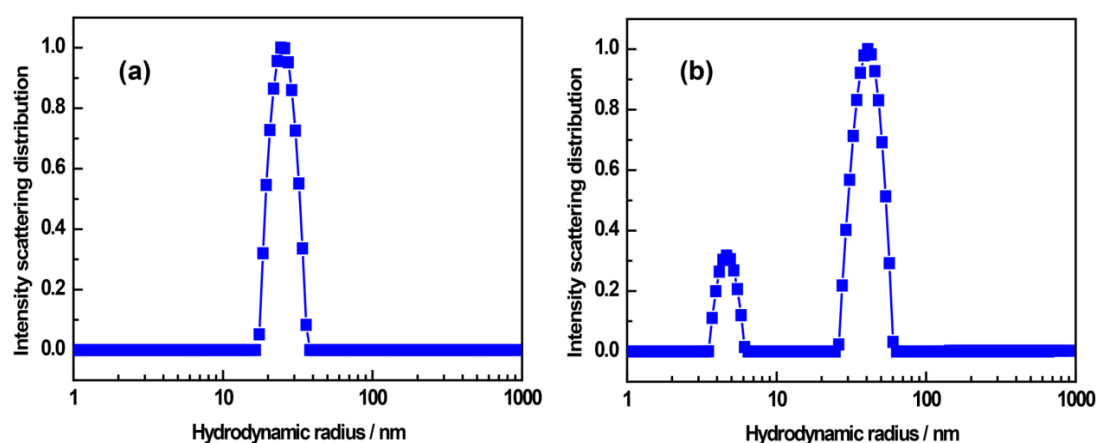
Figure 3.4. CONTIN results for A(B)$_4$ in [C$_4$mim]PF$_6$ (1 wt %) solution at (a) 30 °C and (b) 50 °C under UV light irradiation.
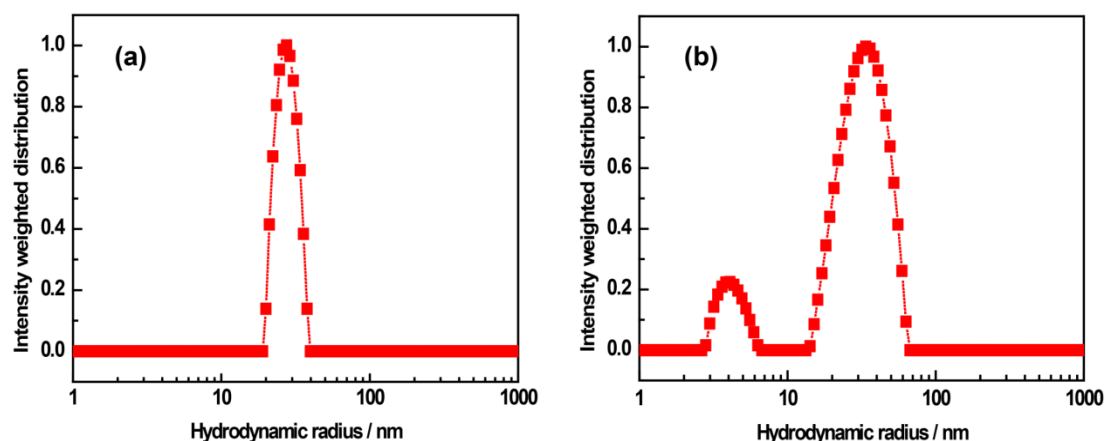
Figure 3.5. CONTIN results for A(B)$_2$ in [C$_4$mim]PF$_6$ (1 wt %) solution at (a) 30 °C and (b) 50 °C under dark conditions.
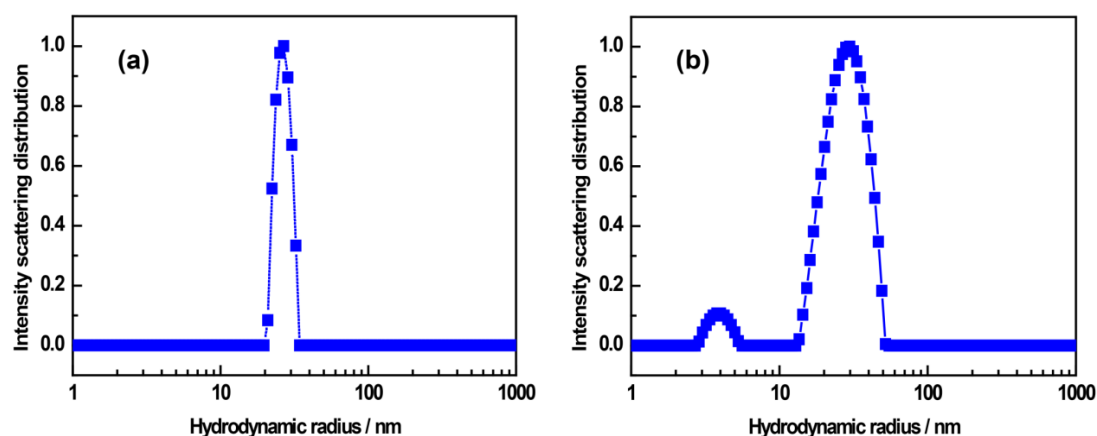
Figure 3.6. CONTIN results for A(B)$_2$ in [C$_4$mim]PF$_6$ (1 wt %) solution at (a) 30 °C and (b) 50 °C under UV light irradiation.

When the temperature was lower than the UCMT, only an intense peak around the R_h of large particles remained and the smaller R_h peak was completely disappeared (**Figure 3.3a**, **3.4a** for A(B)$_4$ and **Figure 3.5a**, **3.6a** for A(B)$_2$). This indicates that unimers aggregated into micelles. For both polymer solutions, the R_h of the micelle at lower temperatures are approximately 25 nm, possibly suggesting core-shell micelles

with solvatophobic P(AzoMA-*r*-NIPAm) core. For A(B)$_4$ polymer solution, the core could be surrounded by solvatophilic tetra-PEG segments that are not free end-arm shells, as they have a tetra-arm nodule in the center of the block copolymer. For A(B)$_2$ polymer solution, the core could also be surrounded by PEG segments. We have previously reported thermo/photoinduced micellization of an azobenzene containing diblock copolymer (PEO-*b*-P(AzoMA-*r*-NIPAm)) in [C$_4$mim]PF$_6$.[9] In that report, below the UCMT, PEO-*b*-P(AzoMA-*r*-NIPAm) diblock copolymers self-assembled into micelles with a solvatophobic P(AzoMA-*r*-NIPAm) core surrounded by a solvatophilic PEO corona of free chains. The size of these micelles was over 100 nm, which is apparently larger than that of the present micelles. This could be attributed to the molecular weight difference between the stimuli-responsive segment and the compatible segment in both copolymers as well as a difference in the block copolymer architecture (simple diblock copolymer and tetra-arm diblock copolymer). In terms of the molecular weight, P(AzoMA-*r*-NIPAm) had 20 kDa and PEO had 15 kDa for the previous diblock copolymer. Conversely, the molecular weights of P(AzoMA-*r*-NIPAm) and PEG for one arm of the present A(B)$_4$ polymer were 11 kDa and 10 kDa, respectively; A(B)$_2$ polymer has molecular weight of 11 kDa for one end block P(AzoMA-*r*-NIPAm) and molecular weight of 20 kDa for midblock PEG. After passing through the UCMT, the scattering intensity monotonically increases (**Figure 3.1a** and **3.2a**), nevertheless, the R_h of the tetra-arm diblock copolymer is almost kept constant with decreasing temperature (**Figure 3.1b** and **3.2b**). Since the scattering intensity is generally proportional to the sixth power of the size of the micelle and

linear to the number of particles. Thus, this result may suggest that the number of particles gradually increases with keeping the size of micelle constant during the cooling process.[7]

The UCMTs of the A(B)$_4$ polymer were 40 °C and 34 °C for the *trans*- and *cis*-form polymer in [C$_4$mim]PF$_6$, respectively (**Figure 3.1b**), for A(B)$_2$ polymer, the UCMTs of *trans*- and *cis*-form polymer were 46 °C and 38 °C, respectively. Importantly, there are 6 °C and 8 °C difference between the UCMT of the *trans*-form polymer and that of the *cis*-form polymer (bistable temperature range) for A(B)$_4$ and A(B)$_2$ polymers, respectively. The UCMT difference comes from the polarity difference of photoisomerization states of AzoMA. It is well-known that the polarity of azobenzene varies with changes in its photoisomerization state; the dipole moment of the planar *trans*- azobenzene (0.5 D) is markedly smaller than that of *cis*-azobenzene (3.1 D).[10] This could result in the higher polarity of the latter and its improved solubility in ILs. The dipole moment (μ) and dielectric constant (ε) of [C$_4$mim]PF$_6$ are reported to be $\mu = 5.3$ D and $\varepsilon = 11.4$, indicating moderate polarity.[10] Therefore, the *trans*-form polymers have higher UCMT in ILs than the *cis*-form polymers. The different temperature ranges between both polymers can be attributed to the difference in azobenzene composition of the block copolymers. The azobenzene composition in the stimuli-responsive segment for A(B)$_4$ polymer was 6.1 mol%, whereas that in A(B)$_2$ polymer was 9.0 mol%. These results are consistent with the previous report on the UCST phase transition of a P(AzoMA-*r*-NIPAm) random copolymer, where the cloud point difference between the *trans*- and *cis*-form

polymers changed from 4 °C to 24 °C with a change in the AzoMA composition (from 1.9 to 8.6 mol%).[9] By using this transition temperature difference, we next demonstrate a photoinduced unimer/micelle transition.

3.2 Unimer-micelle transition of A(B)$_4$ and A(B)$_2$ in [C$_4$mim]PF$_6$ induced by photo-stimuli.

Figure 3.7 and **3.8** show a reversible unimer-micelle transition for A(B)$_4$ and A(B)$_2$ polymer solutions, respectively, induced by light stimuli at a bistable temperature (37 ℃ and 42 ℃ for A(B)$_4$ and A(B)$_2$ respectively). First, A(B)$_4$ and A(B)$_2$ polymer solutions were kept at 37 ℃ and 42 ℃, respectively, under UV light irradiation; the R_h of both polymers was less than 10 nm. The size distribution always displays a bimodal distribution (**Figure 3.9a** and **3.10a**). This is consistent with distribution function of **Figure 3.4b** and **3.6b**. The weight fraction of single polymer chains could also be estimated to be over 0.999, which indicates that aggregation is negligible. At time 0 s, both solutions were irradiated by visible light to form the *trans*-polymer. The size of micelles for both polymers formed by photoinduced transition was approximately 25 nm. This was quite similar to the size of the micelles generated under the thermal-induced transition of both polymers, as shown in **Figure 3.1b** and **3.2b**. The size distribution function exhibits a unimodal distribution (**Figure 3.9b** and **3.10b**), which indicates formation of micelles. There is an induction time (300 s and 400 s for A(B)$_4$ and A(B)$_2$, respectively) for both polymers before aggregation. We previously reported that photoinduced unimer-micelle transition of PEO-*b*-P(AzoMA-*r*-NIPAm) diblock copolymer in an IL required two elementary

steps.[9]
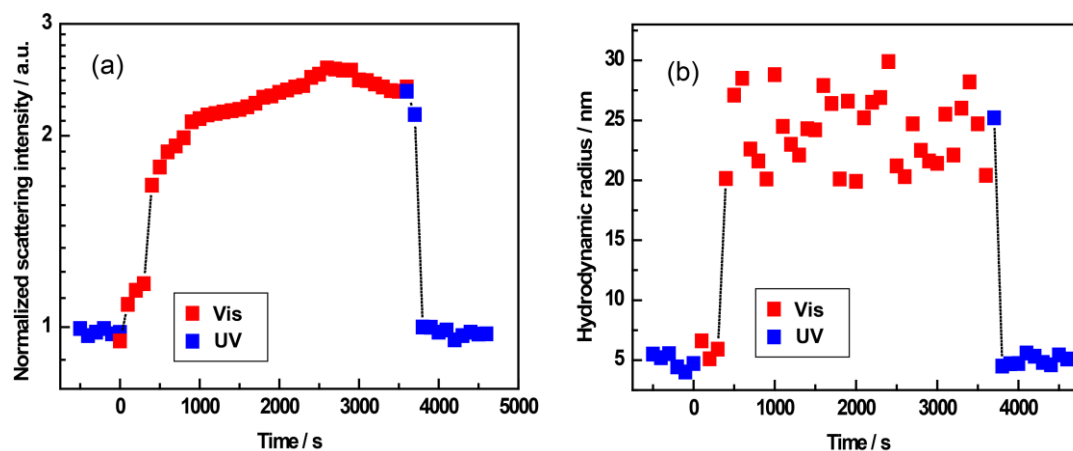
Figure 3.7. Reversible photoinduced self-assembly and dissociation of A(B)$_4$ polymer micelles at 37 °C under UV (blue diamonds) or visible light (red diamonds) irradiation; (a) normalized scattering intensity, (b) mean R_h, as a function of time.
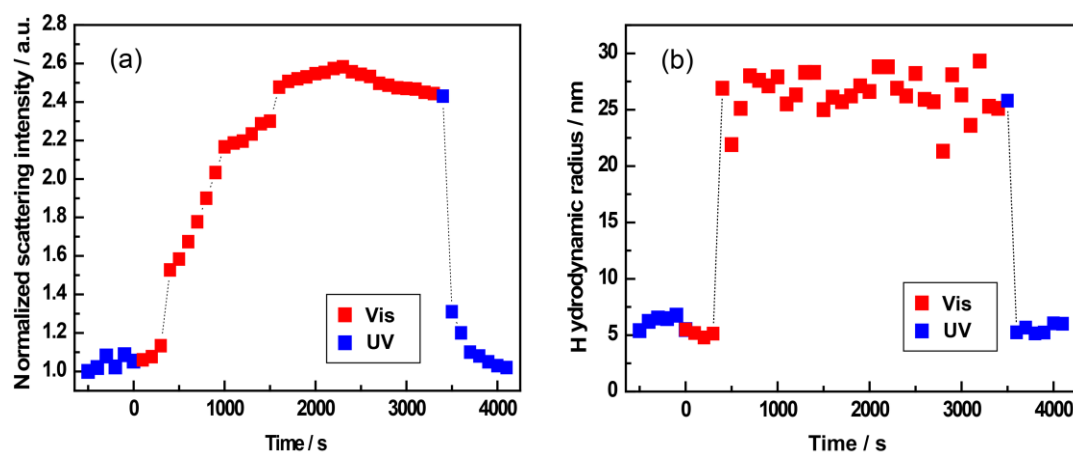
Figure 3.8. Reversible photoinduced self-assembly and dissociation of A(B)$_2$ polymer micelles at 42 °C under UV (blue diamonds) or visible light (red diamonds) irradiation; (a) normalized scattering intensity, (b) mean R_h, as a function of time.
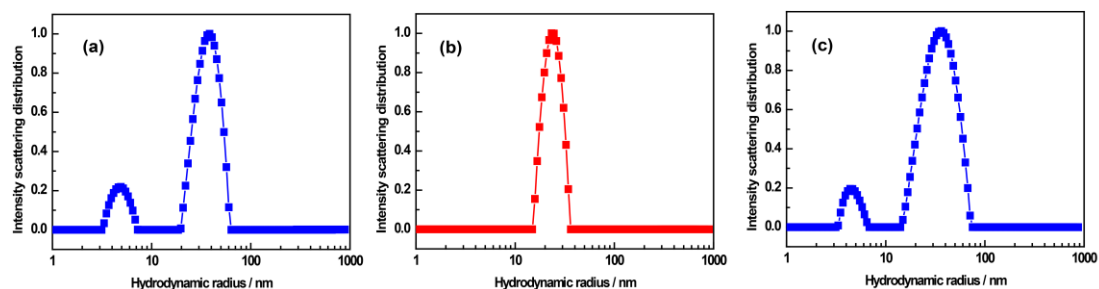
Figure 3.9. CONTIN results for $A(B)_4$ in a [C_4mim]PF_6 (1 wt %) solution at 37 °C: (a) under UV light irradiation (before visible light irradiation), (b) under visible light irradiation, and (c) after switching back to UV light irradiation again.
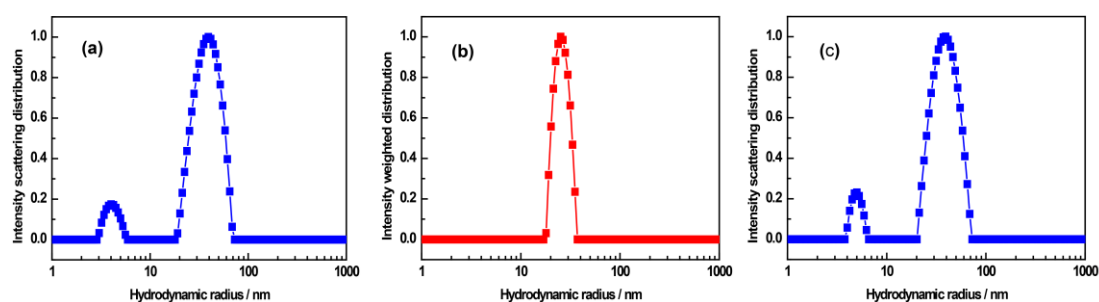
Figure 3.10. CONTIN results for $A(B)_2$ in a [C_4mim]PF_6 (1 wt %) solution at 42 °C: (a) under UV light irradiation (before visible light irradiation), (b) under visible light irradiation, and (c) after switching back to UV light irradiation again.

The first step was the photoisomerization of azobenzene from *cis* to *trans*, while the second step was diffusion of polymers to self-assemble into micelles.[9] We considered these two steps, because photo-induced sol-gel transition for both concentrated polymer solutions at a bistable temperature under visible light irradiation occurred within approximately 100s (**Chapter 4 Figure 4.8**), which mainly induced by photoisomerization of the *cis*- to the *trans*-form of azobenzene within random copolymer blocks, because polymer diffusion can be negligible in concentrated

solution, owing to overlap of polymers in such state. Thus, for diluted polymer solution, polymer diffusion step is the rate-determining step for photoinduced micellization.

After the induction time, the scattering intensity monotonically increased until 2500 s, whilst the average R_h abruptly increased (**Figure 3.7** and **3.8**). Early in the aggregation process, system includes a large amount of unimers and few large aggregates. The scattering intensity strongly depends on the size of particles rather than the number of particles. Therefore, once the unimers aggregation starts, the DLS signal is heavily weighted by the larger particles.[11] Therefore, the increase of scattering intensity from 300 s for A(B)$_4$ and 400 s for A(B)$_2$ to 2500 s is roughly proportional to the increase of the number of micelles. The completion of aggregation process seems to be reached after about 2500 s.

After the micelles were formed under visible light irradiation, we switched back to UV light irradiation at 3400 s and 3300s for A(B)$_4$ and A(B)$_2$, respectively, to form the *cis*-form polymer. Both the scattering intensity and the R_h decreased (**Figure 3.7** and **3.8**). This indicated that the disassociation of micelles into individual single polymer chains, because the UCMT of the *cis*-form polymer was lower than the measurement temperature (37 ℃ and 42 ℃ for A(B)$_4$ and A(B)$_2$, respectively). The distribution function also confirmed this transition (**Figure 3.9c** and **3.10c**). This phenomenon demonstrated that the photoinduced unimer/micelle transition was reversible. The demicellization process was much faster than the micellization process, because no polymer diffusion step was required.

3.3 Conclusions

Firstly, a tetra-arm diblock copolymer (A(B)$_4$) was successfully prepared by RAFT polymerization. The tetra-arm diblock copolymer had tetra-PEG as the solvatophilic central A block and P(AzoMA-r-NIPAm) as four temperature- and photoresponsive end B blocks. For comparison, a triblock copolymer (A(B)$_2$, A: PEG as the solvatophilic midblock, B: P(AzoMA-r-NIPAm)) also be prepared by RAFT polymerization.

Secondly, we investigated phase behavior of A(B)$_4$ and A(B)$_2$ polymers in [C$_4$mim]PF$_6$ under diluted conditions. Temperature dependence of the scattering intensity and hydrodynamic radius from the DLS measurements confirmed that the UCMT of the *trans*-form polymer was 6 °C and 8 °C higher than that of *cis*-form polymer for A(B)$_4$ and A(B)$_2$ polymer, respectively.

Finally, a photoinduced reversible unimer/micelle transition of both polymers utilizing the UCMT difference between the *trans*- and the *ci*s-form polymer in an IL was demonstrated.

3.4 References

1 Iatridi, Z.; Tsitsilianis, C. *Polymers* **2011**, *3*, 1911-1933.

2 Riess, G. *Prog. Polym. Sci.* **2003**, *28*, 1107-1170.

3 Strandman, S.; Zarembo, A.; Darinskii, A. A.; Loflund, B.; Butcher, S. J.; Tenhu, H.
Polymer **2007**, *48*, 7008-7016.

4 He, E.; Ravi, P.; Tam, K. C. *Langmuir* **2007**, *23*, 2382-2388.

5 He, E.; Yue, C. Y.; Tam, K. C. *Langmuir* **2009**, *25*, 4892-4899.

6 Ueki, T.; Yamaguchi, A.; Ito, N.; Kodama, K.; Sakamoto, J.; Ueno, K.; Kokubo, H.;
Watanabe, M. *Langmuir* **2009**, *25*, 8845-8848.

7 Ueki, T.; Yamaguchi, A.; Watanabe, M. *Chem. Commun.* **2012**, *48*, 5133-5135.

8 Shibayama, M.; Karino, T.; Okabe, S. *Polymer* **2006**, *47*, 6446-6456.

9 Ueki, T.; Nakamura, Y.; Lodge, T. P.; Watanabe, M. *Macromolecules* **2012**, *45*,
7566-7573.

10 Hunger, J.; Stoppa, A.; Schrodle, S.; Hefter, G.; Buchner, R. *ChemPhysChem*
2009, *10*, 723-733.

11 Shibayama, M.; Karino, T.; Okabe, S. *Polymer* **2006**, *47*, 6446-6456.

Chapter 4 Thermo-/photo-sensitive ion gels and photo-healable materials

For $A(B)_4$ and $A(B)_2$ polymers in an IL, at low concentrations, $A(B)_4$ and $A(B)_2$ polymers form flower-like micelles, because the looping conformation is preferred.[1] As the concentration increases, a fraction of the midblocks will form bridges between different micellar cores, resulting in the formation of an elastic network.

In this chapter, firstly, we systematically compare gelation characteristics and thermosensitivity of $A(B)_4$ and $A(B)_2$ polymers in $[C_4mim]PF_6$. Secondly, the photo-induced reversible sol-gel transitions are demonstrated at certain temperatures. Finally, photo-healable materials are indicated by using such reversible sol-gel transition.

4.1 Thermoreversible gelation of $A(B)_4$ and $A(B)_2$ in $[C_4mim]PF_6$.

Dynamic shear measurements were performed on $A(B)_4$ and $A(B)_2$ ion gels at 20 wt% polymer concentration in $[C_4mim]PF_6$ under dark conditions over the temperature range of 25-70 °C. Under dark conditions, the azobenzene exists in the *trans*-state ($\approx 100\%$).[2] Representative data at different temperatures are shown in **Figure 4.1a** and **b** for $A(B)_4$ and $A(B)_2$ ion gels, respectively. At 70 °C the both ion gels are viscous liquids. The storage moduli (G') of the both ion gels are clearly lower than their loss moduli (G''), and the both moduli follow different power law in low frequency range: $G' \sim \omega$ and $G'' \sim \omega^2$. This is a typical rheological property of viscoelastic fluid.[3] At 25 °C the both ion gels are in a gel state, G' is significantly

higher than G'', and G' is almost frequency independent. This is a characteristic of solid-like behavior. At intermediate temperatures (A(B)$_4$: 54 °C, A(B)$_2$: 58°C), the both gels show a complicated rheological response. In low frequency window, G' is lower than G'', however G' becomes slightly higher than G'' in high frequency window (G' ≈ G'' ~ $\omega^{0.5}$). This is a typical phenomenon between solid-like and liquid-like states and close to the critical gelation point. These results suggest that the gelation temperature (T_{gel}) for A(B)$_4$ and A(B)$_2$ ion gels is approximately 54 °C and 58 °C, respectively.
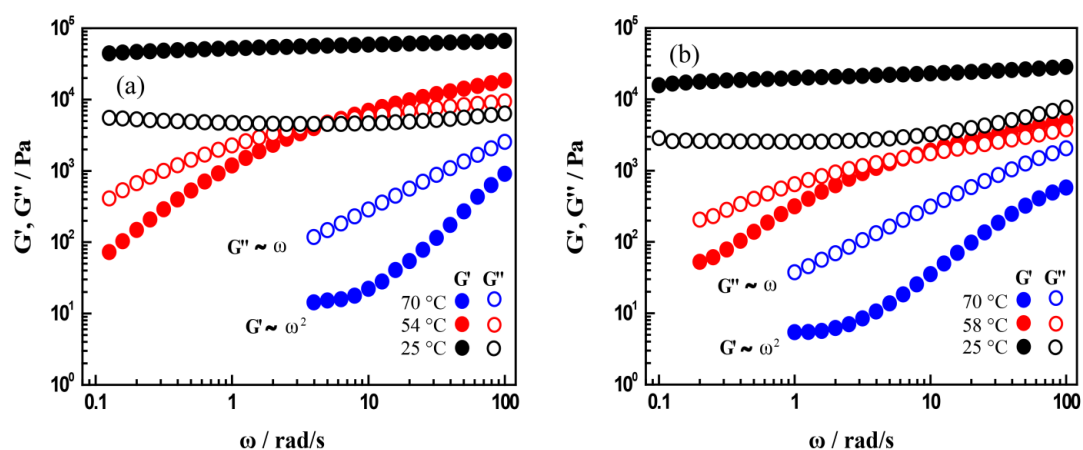
Figure 4.1. Frequency dependences of the dynamic shear moduli (G' and G'') for (a) 20 wt% A(B)$_4$ and (b) 20 wt% A(B)$_2$ solutions in [C$_4$mim]PF$_6$ under dark conditions measured at a strain γ = 1% and three indicated temperatures.

Figure 4.2a and b show thermo-reversible sol-gel transition of 20 wt% A(B)$_4$ and A(B)$_2$ solutions in [C$_4$mim]PF$_6$, respectively. Dynamic shear moduli were measured in the range of 25-70 °C under dark conditions in a heating-to-cooling thermal cycle. At higher temperatures, G' of the both gels is lower than their G'', which indicates that the binary system is in sol state. At lower temperatures, G' of the both gels becomes

higher than their G'', indicating the transition to gel state. There is a crossover of G' and G'' (sol-gel transition) in the heating and cooling processes. For the heating process, the sol-gel transition temperature (T_{gel}) is 55 °C and 59 °C for A(B)$_4$ and A(B)$_2$ ion gels, respectively. For the cooling process, the A(B)$_4$ ion gel has T_{gel} of 54 °C, and T_{gel} of A(B)$_2$ ion gel is 58 °C, which is consistent with the results in **Figure 4.1.** This result demonstrates that thermo-induced sol-gel transition of the both gels is completely reversible. The T_{gel} of A(B)$_2$ ion gel is 4 °C higher than that of A(B)$_4$ ion gel, which can be attributed to higher azobenzene content in A(B)$_2$ polymer (9.0% in A(B)$_2$ and 6.1% in A(B)$_4$). Previously, we reported that phase separation temperatures (T_c) of a series of P(NIPAm-r-AzoMA) in [C$_4$mim]PF$_6$ under dark conditions changed from 75 °C to 85 °C with varying azobenzene content from 1.9% to 8.6%.[4] The both T_{gel} values are lower than T_c of P(NIPAm-r-AzoMA). There are two possible reasons. One explanation is that IL-compatible PEG covalently attached to the random copolymer blocks causes a decrease in T_{gel}.[4] The other reason is molecular weight effect; T_c of PNIPAm decreases with decreasing molecular weight of PNIPAm.[5] The molecular weight of one end block of the both polymers is 11 kDa, however, the reported P(NIPAm-r-AzoMA) has molecular weight of 50 kDa.
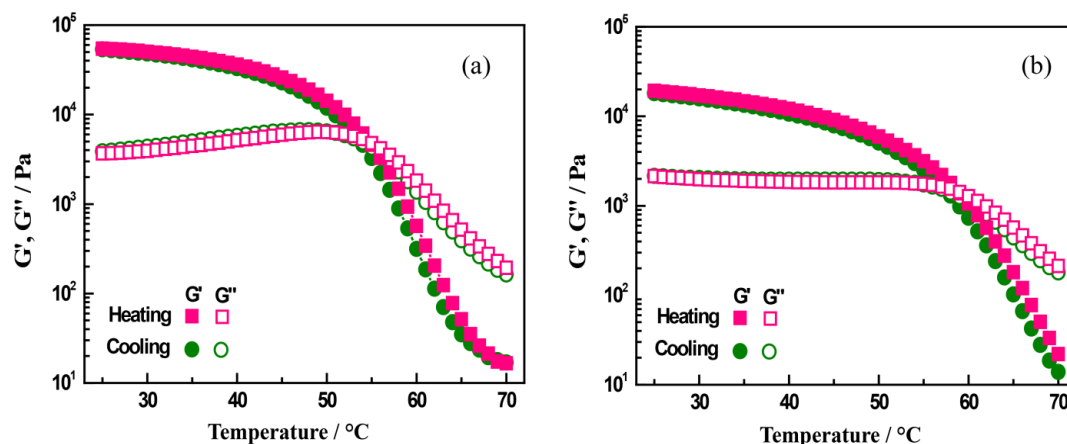
Figure 4.2. Dynamic shear moduli (G' and G'') as a function of temperature measured in a heating-to-cooling thermal cycle for 20 wt% (a) A(B)$_4$ and (b) A(B)$_2$ solutions in [C$_4$mim]PF$_6$ under dark conditions. Measurements were taken at a strain γ = 1% and frequency ω = 6.28 rad/s with heating and cooling rates of ±0.3 °C/min.

4.2 Gelation characteristics of A(B)$_2$ and A(B)$_4$ polymers in [C$_4$mim]PF$_6$.

We compared the gelation properties of A(B)$_4$ with A(B)$_2$ at different polymer concentrations. **Figure 4.3a** and **b** show the temperature dependence of G' and G'' obtained for solutions of A(B)$_4$ and A(B)$_2$ in [C$_4$mim]PF$_6$, respectively, under dark conditions. The both polymers exhibit temperature induced sol-gel transition at all concentrations from 2 wt% to 20 wt%. For the A(B)$_4$ ion gels, gelation is very gradual at concentrations blow 5 wt%, but becomes sharp at higher concentrations than 7 wt%, whereas for the A(B)$_2$ ion gels, gelation does not become sharp until polymer concentration reaches 15wt%. Such broad sol-gel transition has been observed in other thermosensitive A(B)$_2$ hydrogels.[6,7] T_{gel} decreases with a decrease in polymer

concentrations, which is consistent with a previous report on the phase separation temperature of P(AzoMA-*r*-NIPAm).[8] Compared to UCMT of both polymers (40 ℃ and 46 ℃ for A(B)$_4$ and A(B)$_2$, respectively, **Chapter3**, **Figure 3.1** and **3.2**), it is apparent that T_{gel} of both polymer solutions at lower concentration (< 7 wt%) is lower than their UCMT at 1 wt% concentration. This is reasonable considering that UCMT only indicates the start point of chain collapse and aggregation, which were typically measured at low polymer concentrations.[7] For the both polymer solutions, even though the gelation occurred at relatively low concentrations, a self-standing ion gel was obtained at higher polymer concentrations than 3 wt% and 5 wt% for A(B)$_4$ and A(B)$_2$, respectively **(Figure 4.4)**. This result indicates that the critical gelation concentration of self-standing ion gels for A(B)$_4$ is lower than that for A(B)$_2$.
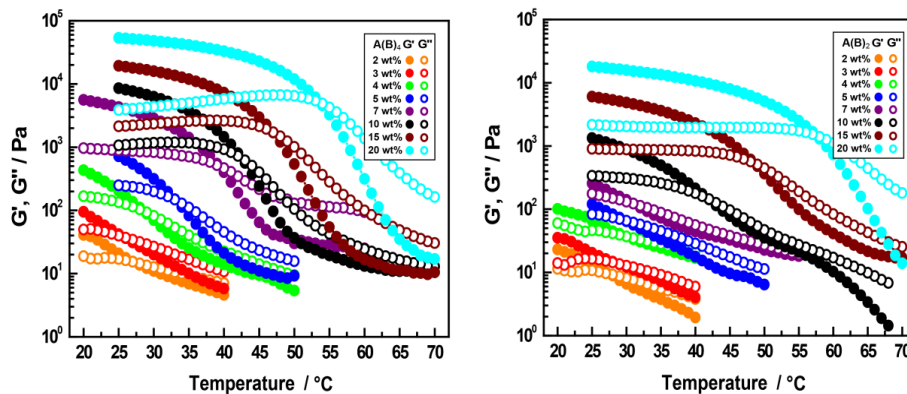
Figure 4.3. Dynamic shear moduli (G' and G'') as a function of temperature measured in a cooling process for A(B)$_4$ and A(B)$_2$ solutions in [C$_4$mim]PF$_6$ at different polymer concentrations under dark condition. Measurements were taken at cooling rates of ±0.3 °C/min. The 20 wt%, 15 wt%, 10 wt% A(B)$_4$ polymer solutions and 20 wt%, 15 wt% A(B)$_2$ polymer solution were measured at a frequency ω = 6.28 rad/s and a strain γ = 1%. The 10 wt% A(B)$_2$ polymer solution was measured at a frequency ω = 6.28 rad/s and a strain decreased linearly from γ = 10% to 5%. The 7 wt% A(B)$_4$ polymer solution was measured at a frequency ω = 10 rad/s and a strain decreased linearly from γ = 40% to 5%. The 7 wt% A(B)$_2$ polymer solution was measured at a frequency ω = 10 rad/s and a strain decreased linearly from γ = 10% to 1%. The 5 wt%, and 4 wt% A(B)$_4$ polymer solutions and 5 wt% A(B)$_2$ polymer solutions were measured at a frequency ω = 10 rad/s and a strain decreased linearly from γ = 20% to 5%. The 4 wt% A(B)$_2$ polymer solutions were measured at a frequency ω = 10 rad/s and a strain decreased linearly from γ = 10% to 1%. The 3 wt% A(B)$_4$ and A(B)$_2$ polymer solution were measured at a frequency ω = 6.28 rad/s and a strain decreased linearly from γ = 30% to 5%. The 2 wt% A(B)$_4$ and 2 wt% A(B)$_2$ polymer solutions were measured at a frequency ω = 6.28 rad/s and a strain decreased linearly from γ = 50% to 5%.
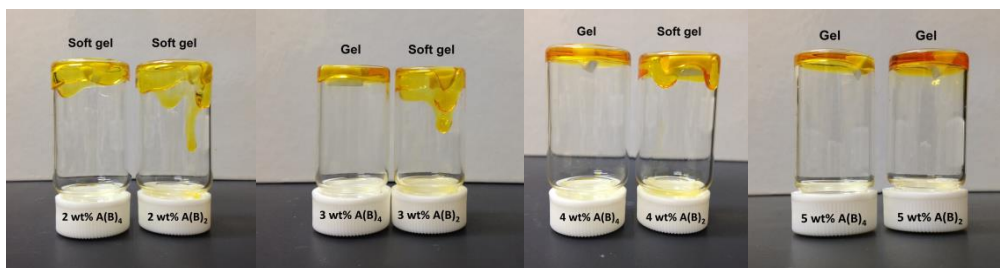
Figure 4.4. Photographs of both $A(B)_4$ and $A(B)_2$ solutions in [C_4mim]PF$_6$ at varying polymer concentrations and 20 °C. Soft gels exhibit solid-like behavior in the rheological measurements, but are not free-standing in the vial upside-down experiments. The pictures were taken at 30 s and 2 min after inverting the vials for 2 wt%, 3 wt% concentrations and 4 wt%, 5 wt% concentrations, respectively.

Figure 4.5 shows the relationship between the magnitude of G' at 25 °C for the both ion gels and polymer concentrations under dark conditions. For the both ion gels, G' increases with increasing polymer concentrations. At the same concentration, the $A(B)_4$ ion gels have apparently higher modulus than the $A(B)_2$ ion gels. A biggest difference was observed at a polymer concentration of 7 wt%, where G' of the $A(B)_4$ ion gel is over 12 times higher than that of the $A(B)_2$ ion gels (**Figure 4.5**). The G' difference between both ion gels depends on the amount of network defects, tanδ value reflect the amount of network defects, the larger tanδ is, the more network defects are. The largest tanδ difference between both ion gels was observed at polymer concentration of 7 wt% (see the blow results in **Figure 4.6**). Thus, the ratio of G' of $A(B)_4$ and $A(B)_2$ ion gels has a maximum at 7 wt% polymer concentration. According to a classical theory, the modulus of rubbery materials is proportional to kT

per elastically effective network strand, that is, $G' = \nu kT$, where ν is the number density of network strands inside the correlation volume and k and T are the Boltzmann constant and the absolute temperature, respectively.[9] If the both ion gels are assumed to be ideal networks with no defects (loops and dangling chains), the ratio of G' of the A(B)$_4$ ion gel to that of the A(B)$_2$ ion gels should be roughly 2, because the A(B)$_4$ structure is equivalent to two A(B)$_2$ polymers that are covalently attached together at the middle of PEG segments. However, all the calculated ratios of G' are apparently higher than 2, indicating that the formation of bridges for A(B)$_4$ is more effective than that for A(B)$_2$, which is consistent with our assumption in the introduction.
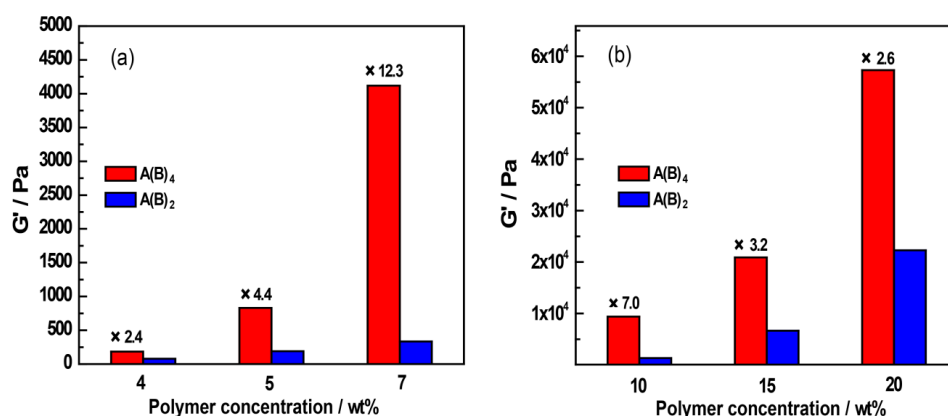
Figure 4.5. Storage modulus (G') of A(B)$_4$ and A(B)$_2$ ion gels at different polymer concentrations, measured at 25 °C under dark conditions. Measurements were taken at a strain $\gamma = 1\%$ and frequency $\omega = 6.28$ rad/s. The value on the top of red column represents G' of A(B)$_4$ ion gels divided by that of A(B)$_2$ ion gels.

Figure 4.6 shows tanδ values at 25 °C for the both ion gels at different concentrations. The value of G' is proportional to the concentration of elastically

effective chains, whereas that of G'' is correlated with the topological defects.[10] Thus, the larger tanδ is, the more network defects are. The tanδ values of A(B)$_4$ ion gels are lower than these of A(B)$_2$ ion gels except the A(B)$_4$ ion gels of 4 wt% concentration. Actually, at concentrations below 4 wt%, A(B)$_4$ ion gels have higher tanδ value than A(B)$_2$ ion gels (data is not shown here), suggesting more network defects for A(B)$_4$ than those for A(B)$_2$, which may be attributed to more compact structure of the star polymers. This compact structure is evident from the GPC traces shown in **Chapter 2**, **Figure 2.4** and **2.5**: both peaks appear at almost the same elution time, though M_n of A(B)$_4$ is twice that of A(B)$_2$. At low concentrations, the formation of defects (especially loops) is inherently more facile for the tetra-arm A(B)$_4$ polymer than the linear A(B)$_2$ polymer. The tanδ values of A(B)$_4$ ion gels become lower than those of A(B)$_2$ ion gels from polymer concentration of 5 wt%, which is the critical concentration for effective suppression of defects in A(B)$_4$ ion gels. These results demonstrate that A(B)$_4$ ion gels have much smaller network defects than A(B)$_2$ ion gels at higher concentrations. In other words, the special architecture of A(B)$_4$ leads to increase in elastically effective chains (bridges), and decrease in ineffective network defects in the ion gels. Therefore, the A(B)$_4$ ion gels have more homogenous network structure than the A(B)$_2$ ion gels at higher concentrations.
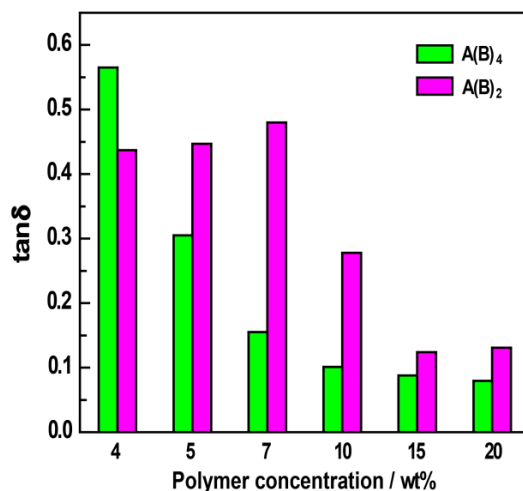
Figure 4.6. Loss tangent, tanδ, of A(B)$_4$ and A(B)$_2$ ion gels at different polymer concentrations, measured at 25 °C under dark conditions. Measurements were taken at a strain γ = 1% and frequency ω = 6.28 rad/s.

4.3 Difference of sol-gel transitions for A(B)$_2$ and A(B)$_4$ in [C$_4$mim]PF$_6$ under visible and UV light irradiation.

Figure 4.7 shows temperature dependent dynamic shear moduli of 20 wt% A(B)$_4$ (**Figure 4.7a**) and A(B)$_2$ (**Figure 4.7b**) in [C$_4$mim]PF$_6$ under visible and UV light irradiation. In the cooling process, the both ion gels under visible and UV light irradiation exhibit similar thermoresponsive sol-to-gel transition to that under dark conditions, as shown in **Figure 4.2**. But the T_{gel} of A(B)$_4$ ion gel under visible and UV light irradiation is 52 ℃ and 48 ℃, respectively. The T_{gel} of A(B)$_4$ ion gel under dark conditions (54 ℃) is the highest (**Figure 4.2a**). The T_{gel} of A(B)$_2$ ion gel follows the order: 58 ℃ (dark) > 55 ℃ (visible) > 49 ℃ (UV). In our previous study, the photostationary *trans*-azobenzene contents in a random copolymer of benzyl

methacrylate and AzoMA were found to be 100%, 85%, and 20% under dark, visible, and UV irradiation, respectively.[11] In other words, we can expect that the T_{gel} values of both ion gels to increase due to increasing *trans*-azobenzene content in the polymers. It is well-known that the polarity of azobenzene depends on photo-isomerization states, i.e., planar *trans*-azobenzene has dipole moment of 0.5 D, while *cis*-azobenzene has dipole moment of 3.0 D. [12] Therefore, in the P(NIPAm-*r*-AzoMA) random copolymer block, *trans*-AzoMA serves as IL-phobic comonomer, while *cis*-AzoMA behaves as IL-philic comonomer, relative to the main monomer NIPAm. Thus, the T_{gel} of both ion gels becomes higher, when contents of *trans*-azobnezene in the polymers become higher. These results show that the T_{gel} of both ion gels depends on photo-isomerization states of the azobenzene in the polymers.

Very importantly, there are temperature differences (ΔT_{gel}) between T_{gel} under visible and T_{gel} under UV light irradiation for the both ion gels. The temperature range from T_{gel} under visible to T_{gel} under UV light irradiation is defined as bistable temperatures. The ΔT_{gel} of the A(B)$_4$ ion gel and that of the A(B)$_2$ ion gel are 4 ℃ and 6 ℃, respectively. The difference in ΔT_{gel} for two polymers can be ascribed to different azobenzene content in the polymers (6.1% and 9.0% for A(B)$_4$ and A(B)$_2$, respectively). This result is consistent with a previous report that phase separation temperature difference between visible and UV light irradiation for a series of P(NIPAm-*r*-AzoMA) polymers increased with increasing azobenzene content in

polymers.[13,14] Next, we further demonstrate photo-induced sol-gel transition by utilizing this temperature difference.
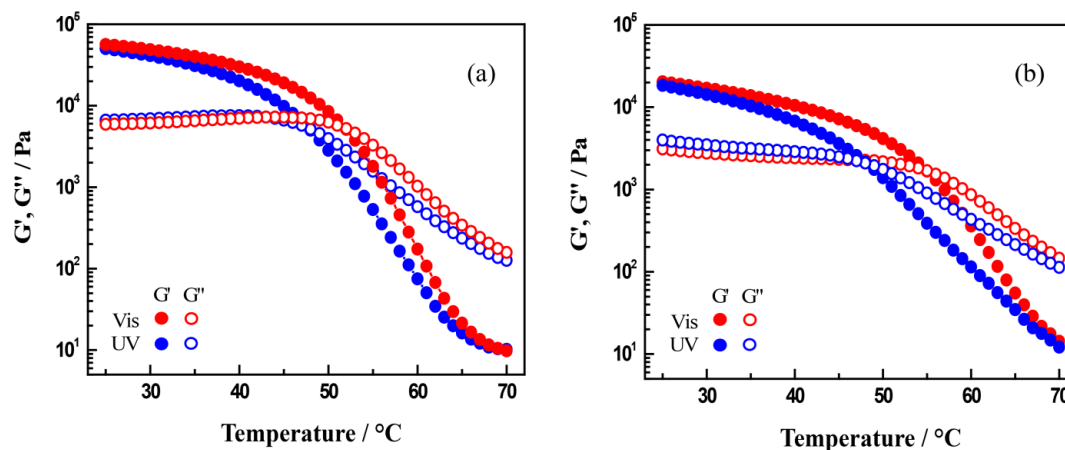
Figure 4.7. Dynamic shear moduli (G' and G'') as a function of temperatures measured under visible light irradiation (red circles) and UV light irradiation (blue circles) for 20 wt% (a) A(B)$_4$ and (b) A(B)$_2$ in [C$_4$mim]PF$_6$. Measurements were taken at a strain $\gamma = 1\%$ and frequency $\omega = 6.28$ rad/s with cooling rates of 0.3 °C/min.

4.4 Photo-induced sol-gel transition.

Figure 4.8a and **b** show dynamic shear moduli of 20 wt% A(B)$_4$ and A(B)$_2$ in [C$_4$mim]PF$_6$ as a function of time, respectively. Measurements were conducted at 50 ℃ and 51 ℃ for A(B)$_4$ and A(B)$_2$, respectively, under visible and UV light irradiation. Under visible light irradiation, *trans*-A(B)$_4$ and *trans*-A(B)$_2$ are dominant, however, under UV light irradiation, *cis*-A(B)$_4$ and *cis*-A(B)$_2$ are dominant. Firstly, A(B)$_4$ and A(B)$_2$ in [C$_4$mim]PF$_6$ were irradiated by visible light to form gel state ($G' >$ G''), which becomes possible because the measurement temperatures are lower than their corresponding T_{gel} under visible light irradiation. At time = 0 s, the visible light

irradiation was switched to UV light irradiation. It is clear from **Figure 4.8a** that G' and G'' decreases with increasing time. For A(B)$_4$, after 900 s, G' becomes lower than G'', indicating that gel-to-sol transition occurs. For A(B)$_2$, after 1000 s, photo-induced gel-to-sol transition occurs. At 3600 s, the UV light visible was switched to the visible light again. After 150 s visible light irradiation (3750 s from the onset) for A(B)$_4$ and after 180 s visible light irradiation (3840 s from the onset) for A(B)$_2$, G' sharply becomes higher than G'', suggesting that the photo-induced sol-to-gel transition happens quickly. After 1400 s visible light irradiation (5000 s from the onset), G' of the both ion gels is recovered to their original values. This result shows that the photo-induced sol-gel transition is completely reversible. The photo-induced sol-to-gel transition process under visible light irradiation is much faster than the photo-induced gel-to-sol transition process under UV light irradiation. A possible reason can be assigned to the difference in the optical density of the materials toward the UV and visible light. The molar absorption coefficient (ε) for $\pi-\pi*$ transition of *trans*-azobenzene at 320-325 nm (ε = 2-3×10^4 L·mol^{-1}·cm^{-1}) is significantly larger than that for n$-\pi*$ transition of *cis*-azobenzene at 440 nm (ε = 1-2×10^3 L·mol^{-1}·cm^{-1}).[15] The UV and visible light that were used here have wavelength of 366 nm and 437 nm, respectively. Thus, under UV light irradiation, the photoisomerization reaction from *trans*- to *cis*-azobenzene gradually occurred from the surface that is close to the UV light source to the bottom of the sample, due to a high ε value of *trans*-azobenzene, however, under visible light irradiation, the photoisomerization reaction from *cis*- to *trans*-azobenzene occurred quickly, thanks to

a lower ε value of *cis*-azobenzene. Therefore, the speed of the photo-induced

sol-to-gel transition is faster than that of the photo-induced gel-to-sol transition.
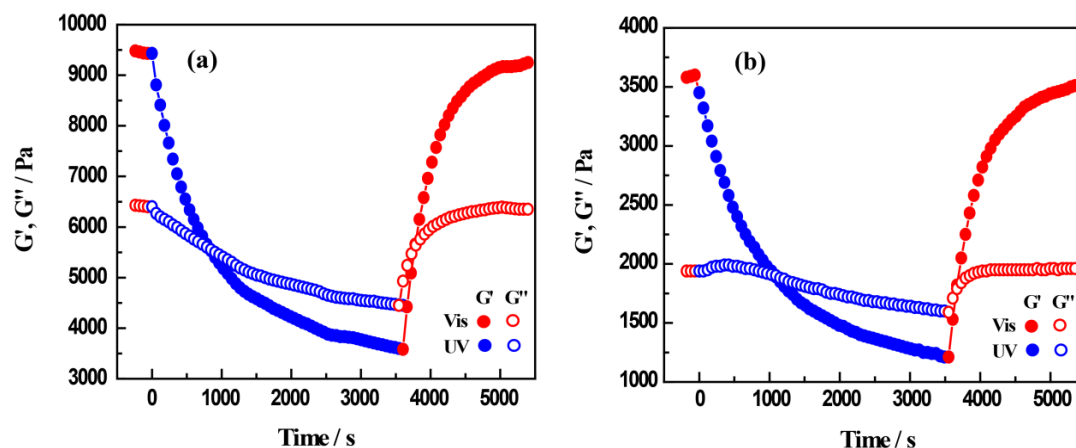
Figure 4.8. Photo-induced sol-gel transition for (a) 20 wt% A(B)$_4$ in [C$_4$mim]PF$_6$ at

50 °C and (b) 20 wt% A(B)$_2$ in [C$_4$mim]PF$_6$ at 51 °C induced by visible (red circles)

and UV (blue circles) light irradiation. Measurements were taken at a strain $\gamma = 1\%$

and frequency $\omega = 6.28$ rad/s.

4.5 Photo-healable ion gels.

Photo-healable ion gels can be realized by utilizing the photo-induced reversible

sol-gel transition phenomena. Photo-healing experiments of the both ion gels were

conducted at 38 ℃ , which is lower than their bistable temperatures. The samples were

too soft at bistabe temperatures for the photo-healing experiments, owing to faster

relaxation of the physical cross-links.[16] Because the ion gels in this study are

viscoelastic samples, the sol-gel transition phenomena are time and temperature

dependent. In order to determine suitable temperatures for the photo-healing

experiments, we firstly analyzed the temperature dependence of relaxation time of the

ion gels, which was obtained by time-temperature superposition of the slower relaxation mode in G' and G''. The time-temperature superposition of G' and G'' of the both ion gels under dark and UV light irradiation (data in **Figure 4.9** and **4.10**) are presented in **Figure 4.11** and **4.12**. Four master curves were obtained. For the both ion gels, at the reference temperatures terminal relaxation times (τ) were determined by the crossover frequency (ω_c) at which the G' and G'' values were equal, and the equation $\tau = 2\pi/\omega_c$. τ of the both ion gels under dark and UV light irradiation at various temperatures are obtained from the shift factor (a_T) (data in **Figure 4.13**) and plotted in **Figure 4.14**. It is found that τ increases with decreasing temperatures, indicating that it takes longer time for the gel-sol transition, which is induced by the relaxation. At the same temperature, τ under UV light irradiation is significantly smaller than that under dark conditions, which is very suitable to realize photo-healable materials. At 40 ℃ , under dark conditions, the $A(B)_4$ and $A(B)_2$ ion gels have τ of 7.80×10^4 s (21.6 h) and 2.09×10^5 s (58 h), respectively. However, at 38 ℃ , under dark conditions, τ for $A(B)_4$ ion gel and $A(B)_2$ ion gel is 6.80×10^5 s (7.8 days) and 1.16×10^6 s (13.4 days), respectively. Thus, we selected 38 ℃ for the photo-healing experiments for the both ion gels. This result is also supported by another experiment, which was conducted at different constant temperatures by direct observation of the change in state of the samples with thickness of 1 mm (same thickness as the photo-healing sample) every 24 h. The experimental results (**Table 4.1)** show the sample shape could be kept for at least 7 days at temperature of 38 ℃ and 36 ℃ . However, the sample flow occurred in the period less than 3 days at

temperatures above 40 ℃. The both experiments indicate that 38 ℃ is a suitable temperature for the photo-healing experiments.
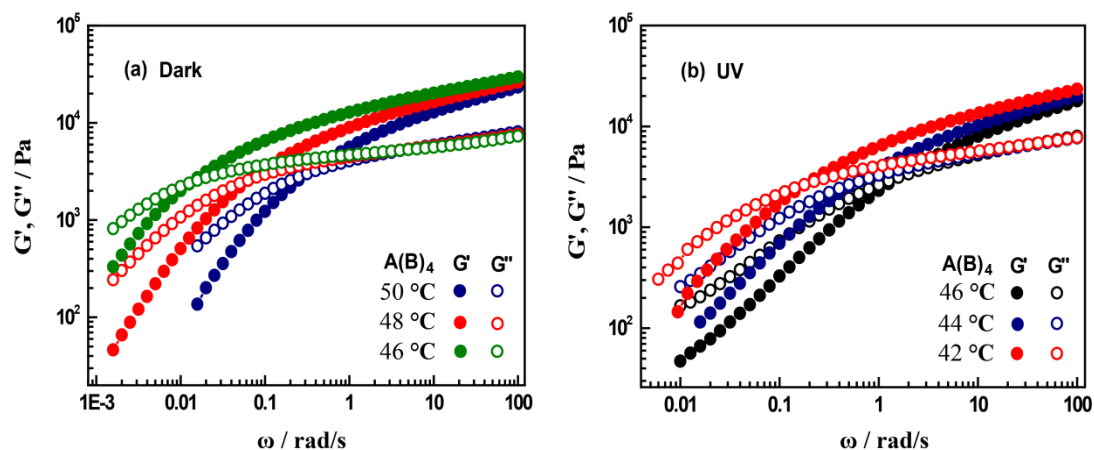
Figure 4.9. Frequency dependences of the dynamic shear moduli (G' and G'') for 20 wt% A(B)$_4$ in in [C$_4$mim]PF$_6$ under dark (a) and UV irradiation (b), measured at strain $\gamma = 1\%$ and three indicated temperatures.
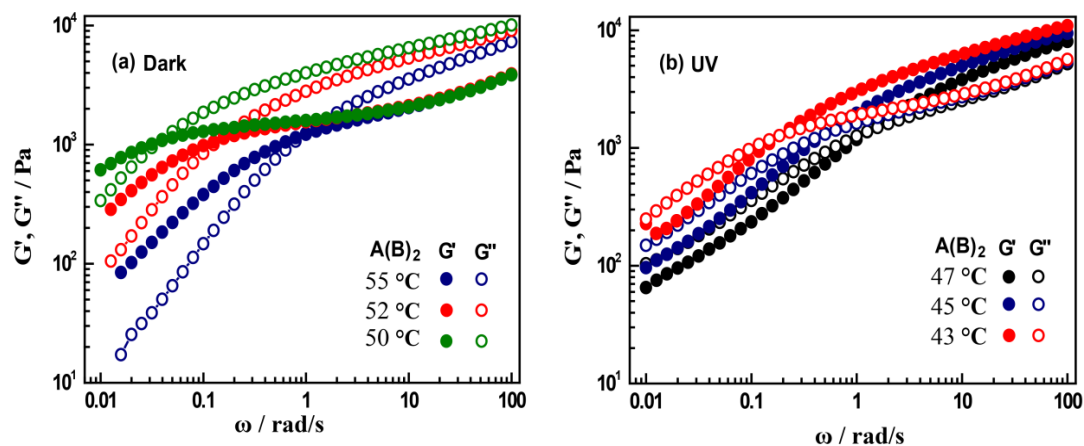
Figure 4.10. Frequency dependences of the dynamic shear moduli (G' and G'') for 20 wt% A(B)$_2$ in [C$_4$mim]PF$_6$ under dark (a) and UV irradiation (b), measured at strain $\gamma = 1\%$ and three indicated temperatures.
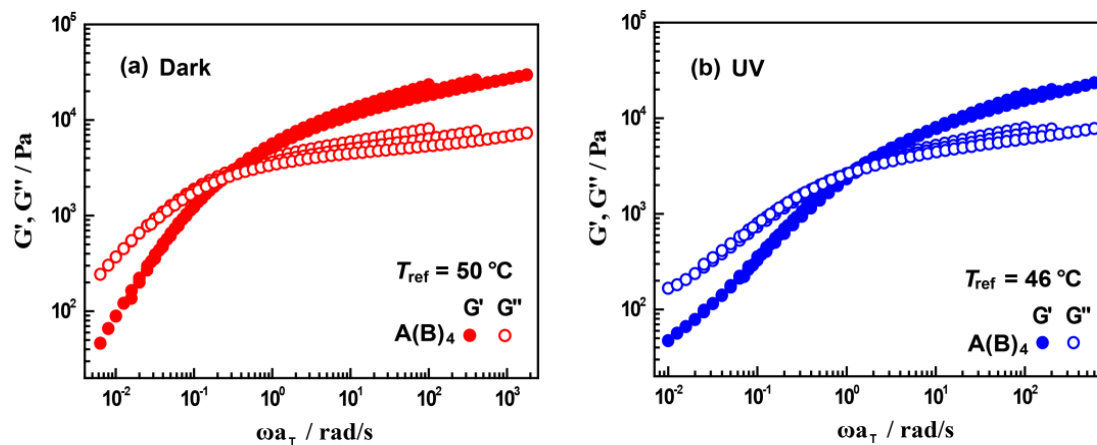
Figure 4.11. Time-temperature superposition of dynamic shear moduli for (G' and G'') for 20 wt% A(B)$_4$ in [C$_4$mim]PF$_6$ under dark (a) and UV irradiation (b). T_{ref} is the reference temperature (data in **Figure 4.9**).
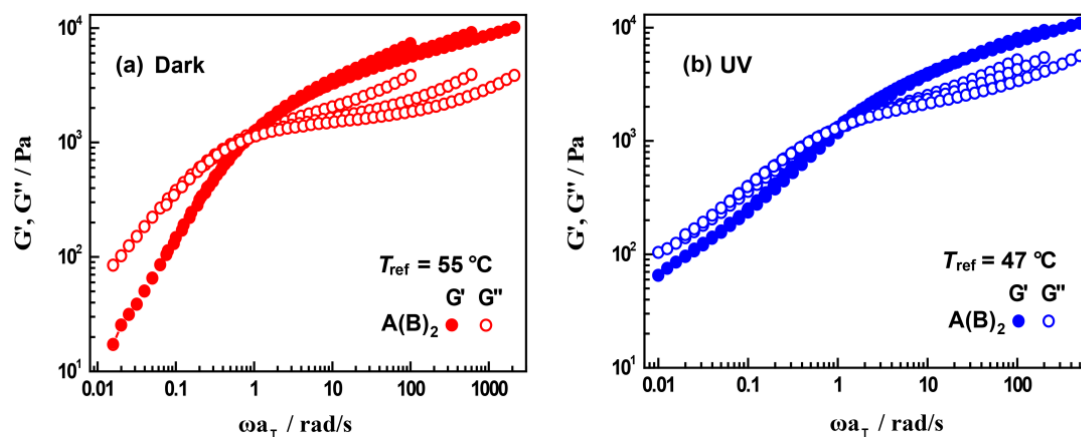
Figure 4.12. Time-temperature superposition of dynamic shear moduli for (G' and G'') for 20 wt% A(B)$_2$ in [C$_4$mim]PF$_6$ under dark (a) and UV irradiation (b). T_{ref} is the reference temperature (data in **Figure 4.10**).
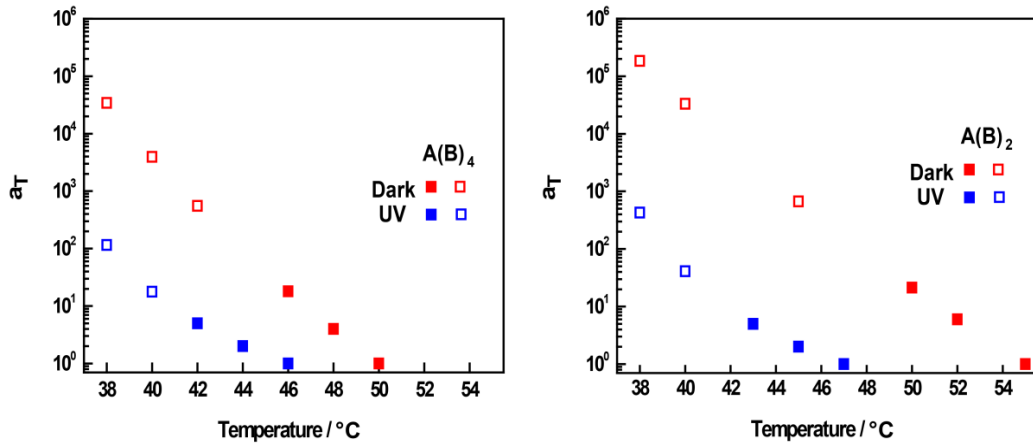
Figure 4.13. Shift factor for the time-temperature superposition for 20 wt% A(B)$_4$ and A(B)$_2$ in [C$_4$mim]PF$_6$ under dark (red squares) and UV irradiation (blue squares). The reference temperature for A(B)$_4$ under dark, T_{ref} = 50 °C and under UV irradiation, T_{ref} = 46 °C; for A(B)$_2$ under dark, T_{ref} = 55 °C and under UV irradiation, T_{ref} = 47 °C. Open squares were obtained from temperature-time superposition.
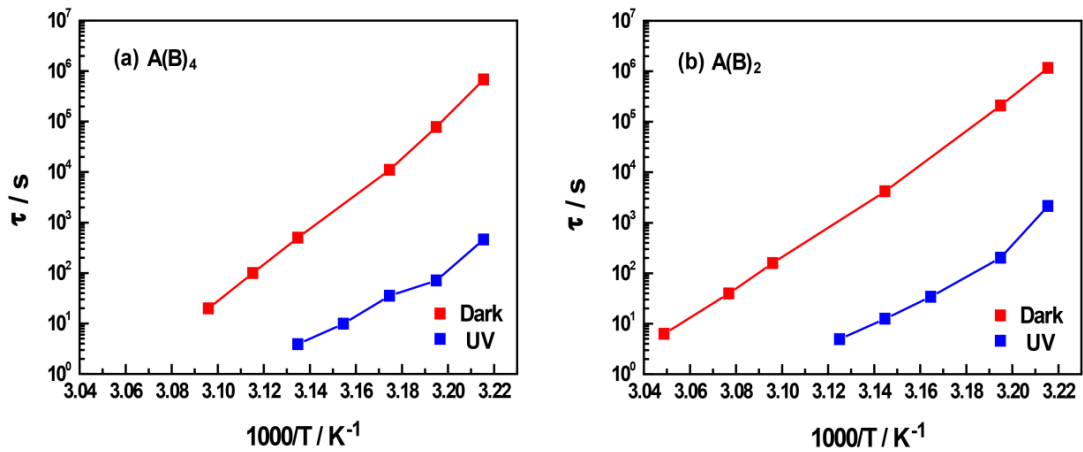
Figure 4.14. Temperature dependence of relaxation times (τ) for 20 wt% A(B)$_4$ (a) and A(B)$_2$ (b) in [C$_4$mim]PF$_6$ under dark (red squares) and UV irradiation (blue squares).

Table 4.1. The relationship between states of ion gels and standing time at different temperatures under dark condition

Ion gel	Temperature / ℃	1 day	2 days	3 days	4 days	5 days	6 days	7 days
20 wt% A(B)$_2$ ion gel	45	Y	-	-	-	-	-	-
	42	Y	-	-	-	-	-	-
	40	N	N	Slightly flow	Y	-	-	-
	38	N	N	N	N	N	N	N
	36	N	N	N	N	N	N	N
20 wt% A(B)$_4$ ion gel	45	Y	-	-	-	-	-	-
	42	Y	-	-	-	-	-	-
	40	Y	-	-	-	-	-	-
	38	N	N	N	N	N	N	N
	36	N	N	N	N	N	N	N

Y and N represents that the ion gel starts to flow and does not flow, respectively, during the indicated period.

As shown in **Figure 4.15**, damaged parts of the ion gels were UV-light-irradiated to induce the gel-to-sol transition, followed by visible-light irradiation to heal the gels by the sol-to-gel transition. It took rather long time to achieve the photo-healing; 50 h UV irradiation for the gel-to-sol transition and 0.5 h visible light irradiation for the

sol-to-gel transition. This result contrasts to the photo-induced gel-to-sol transition process shown in **Figure 4.8**; it took 900 s and 1000 s for the A(B)$_4$ and A(B)$_2$ ion gels, respectively. The difference can be caused by the fact that thickness of the samples for the photo-healing experiments was 1 mm; however, it was 0.2 mm for the rheological measurements. The main reason is that the terminal relaxation time under UV light irradiation at 38 ℃ is much longer than that at a bistable temperature for the experiments in **Figure 4.8**.
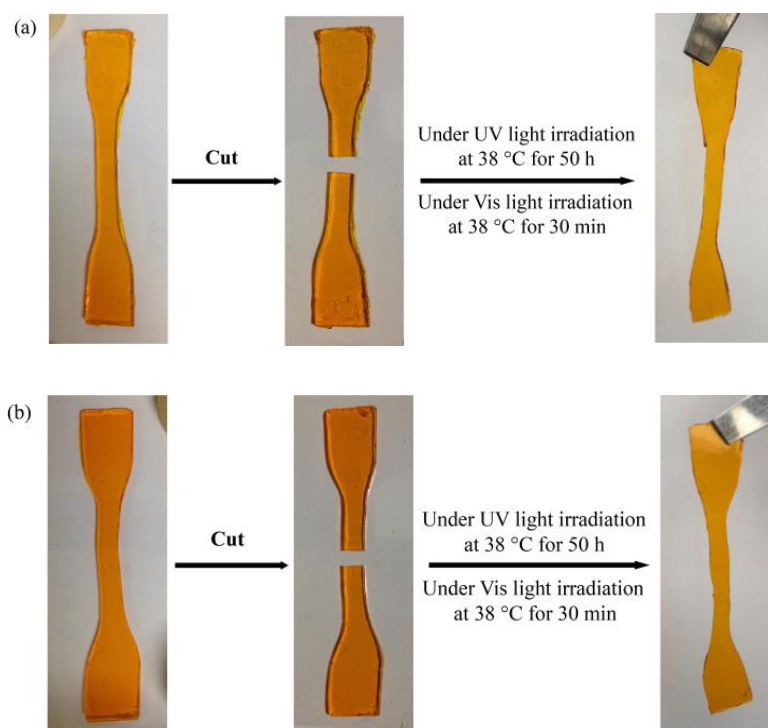
Figure 4.15. Photographs of dumbbell samples of ion gels before and after photo-healing experiments at 38 °C: (a) 20 wt% A(B)$_4$ in [C$_4$mim]PF$_6$ and (b) 20 wt% A(B)$_2$ in [C$_4$mim]PF$_6$.

A stress-strain curve of the A(B)$_4$ ion gel (20 wt% in [C$_4$mim]PF$_6$) is given in **Figure 4.16**. For the A(B)$_4$ ion gel, the photo-healed sample exhibits almost the same mechanical properties as original one. Photo-healing efficiency was calculated by comparing mechanical properties before and after the photo-healing experiments. These data are shown in **Table 4.2** for the A(B)$_4$ and A(B)$_2$ ion gels. For the A(B)$_4$ ion gel, the photo-healing efficiency of the tensile strength is as high as 80%, the photo-healing efficiency of the modulus reaches 79%, and the elongation at the break was recovered completely, indicating that the damage to the sample was almost perfectly healed. On the other hand, for the A(B)$_2$ ion gel, the tensile strength, the modulus, and the elongation at break was less recovered by the same photo-healing conditions, compared with the A(B)$_4$ ion gel. Although the photo-healed sample of the A(B)$_2$ ion gel was visually checked and showed no obvious damage, small cracks may still exist inside. Possibly, the A(B)$_2$ ion gel may need a much longer photo-healing time to complete the healing process. The terminal relaxation times at 38 °C under UV light irradiation are 460 s and 2136 s for the A(B)$_4$ and A(B)$_2$ ion gels, respectively. Thus, the A(B)$_2$ ion gel appear to exhibit relative lower photo-healing efficiency. For the both original samples, **Table 4.2** also shows that A(B)$_4$ ion gel has much higher mechanical properties than A(B)$_2$ ion gel, which is consistent with the result shown in **Figure 4.3**.
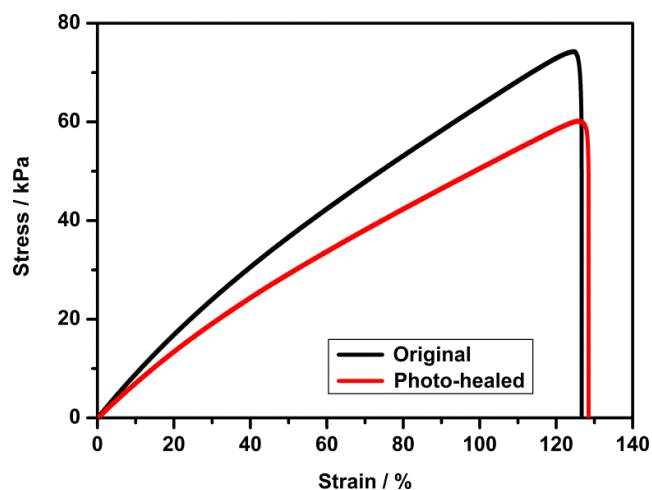
Figure 4.16. Stress-strain curves of the $A(B)_4$ ion gel (20 wt% in $[C_4mim]PF_6$). Measurements were taken at room temperature and the elongation speed was 6 mm/min.

Table 4.2. Mechanical properties of both ion gels

Ion gel		Tensile strength / kPa	Elastic modulus / kPa	Elongation at break / %
$A(B)_4$	Original	74	189	126
	Photo-healed	60	149	128
	Photo-healing efficiency	81%	79%	101%
$A(B)_2$	Original	24	44	71
	Photo-healed	17	30	47
	Photo-healing efficiency	71%	68%	66%

4.6 Conclusions

We demonstrated a strategy on the suppression of network defects and improving mechanical properties for physical ion gels based on block copolymers by utilizing gelation of a tetra-arm diblock copolymer in an IL. Comparing with a conventional method on improving mechanical properties of a triblock copolymer ion gels by introducing chemical cross-links into the endblock microdomains, our approach had a merit that the mechanical properties were improved and meanwhile the reversible sol-gel transition remained. The same principle can be extended to other gel systems as well.

Ion gels from a tetra-arm diblock copolymer (A(B)$_4$: A block is tetra-PEG, B block is P(AzoMA-r-NIPAm)) had more uniform networks, lower critical gelation concentration for obtaining a self-standing gel, and higher modulus, as compared to a triblock copolymer (A(B)$_2$: A block: PEG, B block is P(AzoMA-r-NIPAm)) ion gels.

The A(B)$_4$ ion gels showed thermo-reversible sol-gel transition, and the gelation temperature depended on photoisomerization states of the azobenzene moiety in the polymers. At a bistable temperature, photo-induced sol-gel transition was completely reversible. Photo-healable ion gels could be realized by using such reversible transition. The photo-healing efficiency was higher than 80%, indicating this possess exhibits an efficient healing property.

4.7 References

1 Balsara, N. P.; Tirrell, M.; Lodge, T. P. *Macromolecules* **1991**, *24*, 1975-1986.

2 Ueki, T.; Yamaguchi, A.; Ito, N.; Kodama, K.; Sakamoto, J.; Ueno, K.; Kokubo, H.; Watanabe, M. *Langmuir* **2009**, *25*, 8845-8848.

3 Larson, R. G. *The Structure and Rheology of Complex Fluids*; Oxford University Press: New York, 1999.

4 Ueki, T.; Nakamura, Y.; Lodge, T. P.; Watanabe, M. *Macromolecules* **2012**, *45*, 7566-7573.

5 Ueki, T.; Watanabe, M. *Chem. Lett.* **2006**, *35*, 964-965.

6 Gu, Y.; Zhang, S.; Martinetti, L.; Lee, K.-H.; McIntosh, L. D.; Frisbie, C. D.; Lodge, T. P. *J. Am. Chem. Soc.* **2013**, *135*, 9652-9655.

7 Ge, Z.; Zhou, Y.; Tong, Z.; Liu, S. *Langmuir* **2011**, *27*, 1143-1151.

8 Ueki, T.; Nakamura, Y.; Yamaguchi, A.; Niitsuma, K.; Lodge, T. P.; Watanabe, M. *Macromolecules* **2011**, *44*, 6908-6914.

9 Rubinstein, M.; Colby, R. H. Polymer Physics, Oxford University Press, New York, 2003

10 Sakai, T.; Akagi, Y.; Matsunaga, T.; Kurakazu, M.; Chung, U.-I.; Shibayama, M. *Macromol. Rapid Commun.* **2010**, *31*, 1954-1959.

11 Ueki, T.; Yamaguchi, A.; Ito, N.; Kodama, K.; Sakamoto, J.; Ueno, K.; Kokubo, H.; Watanabe, M. *Langmuir* **2009**, *25*, 8845-8848.

12 Kumar, G. S.; Neckers, D. C. *Chem. Rev.* **1989**, *89*, 1915-1925.

13 Rodriguez, H.; Rogers, R. D. *Fluid Phase Equilib.* **2010**, *294*, 7-14.

14 Ueki, T.; Nakamura, Y.; Lodge, T. P.; Watanabe, M. *Macromolecules* **2012**, *45*, 7566-7573.

15 Tamai, N.; Miyasaka, H. *Chem. Rev.* **2000**, *100*, 1875-1890.

16 He, Y.; Lodge, T. P. *Macromolecules* **2008**, *41*, 167-174.

Chapter 5 Summary and Outlook

5.1 Summary

The objective of this thesis research is to study self-assembly of tetra-arm diblock copolymer in IL under diluted conditions and achieve block copolymer physical ion gels with high mechanical properties and smaller network defects. First of all, a tetra-arm diblock copolymer ([PEG-P(AzoM-r-NIPAm)]$_4$) (A(B)$_4$) was successfully prepared by RAFT polymerization. The tetra-arm diblock copolymer had tetra-PEG as the solvatophilic central block and P(AzoMA-r-NIPAm) as four temperature- and photoresponsive end blocks. A triblock copolymer (P(AzoM-r-NIPAm)-PEG-P(AzoM-r-NIPAm)) (A(B)$_2$) also be prepared by RAFT polymerization for comparison.

Secondly, We studied their self-assembly in [C$_4$mim]PF$_6$ under diluted conditions. It was shown that the UCMT of the *trans*-form polymer was 6 ℃ and 8 °C higher than that of *cis*-form polymer for A(B)$_4$ and A(B)$_2$, respectively, from the DLS measurements. A photoinduced reversible unimer/micelle transition of the both polymers utilizing the UCMT difference between the *trans*- and the *cis*-form polymer in [C$_4$mim]PF$_6$ was demonstrated.

Thirdly, We demonstrated a strategy on the suppression of network defects and improving mechanical properties for physical ion gels based on block copolymers by utilizing gelation of a tetra-arm diblock copolymer in an IL. The same principle can be extended to other gel systems as well. Ion gels from a tetra-arm diblock copolymer

had more uniform networks, lower critical gelation concentration for obtaining a self-standing gel, and higher modulus, as compared with a triblock copolymer ion gels.

Finally, the A(B)$_4$ ion gels showed thermo-reversible sol-gel transition, and the gelation temperature depended on photoisomerization states of the azobenzene moiety in the polymers. At a bistable temperature, photo-induced sol-gel transition was completely reversible. Photo-healable ion gels could be realized by using such reversible transition. The photo-healing efficiency was higher than 80%, demonstrating this ion gel exhibits an efficient healing property.

5.2 Outlook

Self-assembly of other star shape block copolymers in ILs is an interesting research flied, because the knowledge of self-assembly of other star block copolymers is still rare in ILs up to now. Therefore, it is necessary to further study the relationship between ordered structure of micelles and architecture of block copolymers to precisely control structure of nanomaterials at the microscopic level. For block copolymer ion gels, it is interesting to study the relationship between mechanical properties of ion gels and architecture of block copolymers and the relationship between mechanical properties of ion gels and microscopic ordered structure of block copolymers in concentration solutions. Because the mechanical properties of materials not only depend on chemical structure of polymers but also are related to the microscopic order structure of polymer in bulk or in concentration solutions. Thus, in

the future, the detailed structure of both polymer ion gels will be determined by small angle X-ray scattering (SAXS). About photo-healable materials, other healable materials will be developed by using other healing ways, such as ionic interaction, hydrogen bonding and dynamic covalent bond. The concept in realizing photo-healable materials could be extended into other functional materials, such as photo-induced actuator.

List of publications

1. **X. Ma**, R. Usui, Y. Kitazawa, H. Kokubo and M. Watanabe. Temperature and Light Induced Self-Assembly Changes of a Tetra-Arm Diblock Copolymer in an Ionic Liquid. *Polymer Journal*, doi:10.1038/pj.2015.55.
2. **X. Ma**, R. Usui, Y. Kitazawa, H. Kokubo and M. Watanabe. Photo-Healable Ion Gel with Improved Mechanical Properties Using a Tetra-Arm Diblock Copolymer in an Ionic Liquid. *Polymer*, doi:10.1016/j.polymer.2015.09.058.

International and domestic conferences

International conferences

1. **X. Ma**, R. Usui, Y. Kitazawa, H. Kokubo and M. Watanabe. The 6th International Congress on Ionic Liquids, June 16-20, 2015, Jeju, Korea.
2. **X. Ma**, R. Usui, Y. Kitazawa, H. Kokubo and M. Watanabe. The joint symposium of the 22nd Polymer Networks Group Meeting (PNG) and the 10th Gel Symposium, November 10-14, 2014, Tokyo University, Japan.

Domestic conferences

1. **X. Ma**, R. Usui, Y. Kitazawa, H. Kokubo and M. Watanabe. The 6th Ionic Liquid Symposium, October 26-27, 2015, Kyoto, Japan.
2. **X. Ma**, R. Usui, Y. Kitazawa, H. Kokubo and M. Watanabe. The 64th SPSJ Annual Meeting, May 27-29, 2015, Hokkaido, Japan.
3. **X. Ma**, R. Usui, Y. Kitazawa, H. Kokubo and M. Watanabe. The 26th Symposium on Polymer Gels. January 19-20, 2015, Tokyo University, Japan.
4. **X. Ma**, R. Usui, Y. Kitazawa, H. Kokubo and M. Watanabe. Gel Workshop, September 26-27, 2014, Nagasaki, Japan.
5. **X. Ma**, R. Usui, Y. Kitazawa, H. Kokubo and M. Watanabe. The 63th Symposium on Macromolecules, 2014, September 24-26, Nagasaki, Japan.
6. **X. Ma**, R. Usui, Y. Kitazawa, H. Kokubo and M. Watanabe. The 63th SPSJ Annual Meeting, May 28-30, 2014, Nagoya, Japan.